Artificial enzymes for Diels-Alder reactions

Wadih Ghattas, Jean-Pierre Mahy, Marius Réglier, A. Jalila Simaan

Artificial enzymes for Diels-Alder reactions

Wadih Ghattas,*[a] Jean-Pierre Mahy,[a] Marius Réglier,[b] and A. Jalila Simaan*[b]

Dedicated to the memory of Professor Bernard Waegell

[a] Dr. W. Ghattas, Prof. J.-P. Mahy
Institut de Chimie Moléculaire et des Matériaux d'Orsay (ICMMO) UMR 8182 CNRS - Univ Paris Sud, Université Paris-Saclay
Orsay 91405 Cedex, France
E-mail: wadih.ghattas@u-psud.fr
[b] Dr. A. J. Simaan, Dr. M. Réglier
Aix Marseille Univ, CNRS, Centrale Marseille, iSm2, Marseille, France.
E-mail: jalila.simaan@univ-amu.fr

Abstract

Diels-Alder (DA) reaction is a cycloaddition of a conjugated diene and an alkene (dienophile) leading to the formation of a cyclohexene derivative *via* a concerted mechanism. As DA reaction generally proceeds with a high degree of regio- and stereoselectivity, it is widely used in synthetic organic chemistry. Considering eco-conscious public and governmental movements, efforts are directed towards the development of industrial processes that meet environmental concerns. Artificial enzymes, that can be developed to catalyze abiotic reactions, appear as important synthetic tools of synthetic biology field. This review describes the different strategies used for developing protein -based artificial enzymes for DA reaction, including for *in cellulo* approaches.

1. Introduction

1.1. Context

Our growing concerns about the limited petroleum resources and environmental problems are pushing chemists to develop processes increasingly respectful of the environment and using renewable resources. Synthetic biology, with the use of microorganisms as cell factories, is one tool to reach this demand.[1-3] In order to achieve this goal, the scope of biocompatible reactions has to be extended. Artificial enzymes coming from activity-repositioned or refashioned proteins, or *de novo* created enzymes, are among the main synthetic tools of the new age of chemistry.[4] Artificial enzymes development is in line with recent progresses including chemoenzymatic processes, multi-step processes, enzyme evolution techniques facilitating applications under harsh industrial conditions, enzyme immobilization tools, metabolic pathway engineering as well as *in cellulo* / *in vivo* catalysis to produce fine chemicals.[5,6] *In vivo* catalysis by artificial enzymes is therefore a challenging new leap for their applications which has been targeted in the last few years.[7-10] In recent years, a growing number of artificial enzymes have emerged. Among them, artificial enzymes that catalyze a Diels-Alder (DA) reaction[11] have received particular attention since, until the end of the 20th century, DA reactions were believed to belong to the sole domain of chemistry and introducing them into the biocatalysis panoply represented an important challenge.

1.2. Diels-Alder reaction

DA is an emblematic reaction that has not only marked synthetic chemistry[12,13] but also biology as it is becoming an important tool for site-selective protein chemical modification for probing and controlling protein functions *in vitro* and in living systems.[14] DA reaction is a [4+2]-cycloaddition of a conjugated diene and an alkene (dienophile) that leads to the formation of a substituted cyclohexene derivative (Homo-DA, Figure 1). An interesting feature of DA reactions is the formation of heterocyclic compounds by cycloadditions of dienes and dienophiles which contain at least one heteroatom (Hetero-DA, Figure 1).

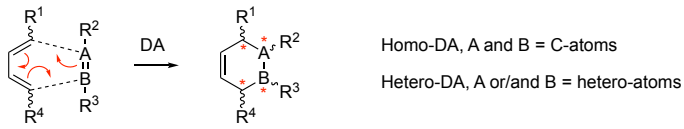

Figure 1. General DA reactions.

The main DA reaction's value lies in the ability to create, in one step, four stereogenic centers which relative configurations arise from the stereochemistry (*E vs. Z*) of the precursors and the geometry (*exo vs. endo*) of the transition state (TS). DA reaction is a concerted thermal pericyclic reaction of the 4 π-electrons of the diene and the 2 π-electrons of the dienophile. Regio- and stereochemistry of DA reactions are governed by the Woodward-Hoffmann rules that imply the symmetry conservation of the frontier orbitals (HOMO and LUMO) (Figure 2B and C).[15] In normal electron-demand DA reactions, with a dienophile substituted by an electron-withdrawing group (EWG, Z) and a diene bearing an electron-donating group (EDG, Ẍ), the HOMO of the diene overlaps with the LUMO of dienophile in a suprafacial interaction. In this case, the main product of the cycloaddition is the *ortho*-adduct (Figure 2A). This preference for the *ortho*-adduct over the *meta*-adduct can be explained considering the coefficients of the atomic orbitals of the HOMO and LUMO. The largest coefficient of the diene HOMO is on the C_γ-atom and that of the dienophile LUMO is located on the C_β-atom. As the favored TS is the one involving overlap of the largest atomic orbital coefficients, the formation of the *ortho*-adduct is preferred. (Figure 2C).[16] Among the ortho adducts, formation of the endo-adduct is kinetically favored due to favorable secondary orbital interactions that

stabilize the transition state (Figure 2C). To increase the reaction kinetics, Brönsted or Lewis acids that lower the energy of the dienophile LUMO have been widely utilized in catalyzed-DA reaction (Figure 2B).[17] Electrostatic effects decreasing the activation energy of DA reactions have also been used in an organocatalytic approach.[18] In bulk aqueous solution, acceleration of DA reactions by hydrophobic containment[19] was achieved in zeolite[20] or using macrocyclic molecules such as cyclodextrins,[21] calixarenes[22] and cucurbiturils.[23] DA reactions have also been the subject of important developments in asymmetric synthesis with the use of chiral auxiliary on the reactants or chiral ligands in metal-catalyzed DA reactions.[24] In this context, Jäschke with RNA[25], Feringa and Roelfes with DNA[26] and G-quadruplex DNA[27] anchoring a metallic cofactor introduced the concept of RNA/DNAzymes that provided efficient catalysts in enantioselective DA reactions.[28-30]

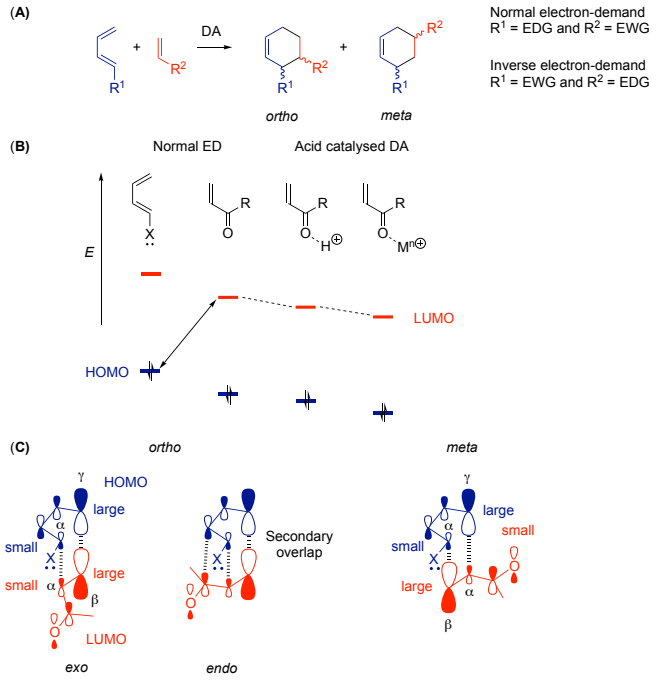

Figure 2. DA reaction (**A**) Regiochemistry; (**B** and **C**) Frontier orbitals HOMO and LUMO involved in normal electron-demand DA reaction (Ẍ = EDG)

1.3. Natural Diels-Alderases

Until the end of the last century, it was believed that DA reactions only belonged to the domain of synthetic chemistry. However in 2000, Vederas[31] and Watanabe[32] reported for the first time in the literature two multifunctional enzymes displaying Diels-Alderase (DAase) activities. In 2011, the first stand-alone DAase, SpnF, was discovered by the group of Liu[33] opening the way to the discovery of other DAases.[34-40] While over the last 20 years, a growing number of putative DAases has been reported,[41] few of them were clearly identified as DAases and the debate regarding the degree of concertedness for the formation of the two C–C bonds remains opened. Until recently, DAases reported in the literature only catalyzed intramolecular cycloadditions. Recently, a DAase catalyzing intermolecular DA reactions, was reported in the literature (MADA).[42] MaDA is involved in the biosynthesis of the natural isoprenylated flavonoid chalcomoracin with a high efficiency and enantioselectivity. Interestingly, MaDA exhibits substrates promiscuity towards both dienes and dienophiles, offering opportunities for enzyme evolution towards the utilization of non-natural substrates.

X-ray structures of several natural DAases were reported (LepI,[43] MaIC,[44] Spnf,[45] AbyU,[46] PyrI4,[47] and PyrE3[48], MaDA[42]). In most cases,[i] X-ray structures indicate that these enzymes act as *entropy traps*[49] binding the substrates into a hydrophobic pocket and forcing the diene and dienophile to adopt a conformation close to the one of the TS.

In addition, theoretical investigations (QM/MM, MD) have suggested that within the cavity, electrostatic effects contribute to the polarization of the diene and the dienophile lowering the activation enthalpy due to a stabilization of charge redistributions in the TS.[46] While, 3D structures point to residues involved in the fixation/activation of the substrates, site-directed mutagenesis of these residues have never completely eliminated the DAase activities so far. This is illustrated by the example of PyrI4. The crystallographic structure of PyrI4 was solved in the presence of the DA reaction product that lies in an hydrophobic cavity with Gln115 and His117 residues that appear to be responsible for the activation of the dienophile precursor (Figure 3).[47] Mutation of Gln115 and His117 into alanines resulted respectively in only 30% and 6% decrease in enzymatic activity (k_{cat}), without significant influence in substrate-binding affinity (K_M). This was attributed to the presence of other stabilizing interactions and to the flexibility of a *N*-terminal lid which imposes conformational constraints and enhances the activation of the substrates. Although structural and mutagenesis data are not yet available for all enzymes, the plasticity of the protein pocket seems to be a shared feature of natural DAases.

The knowledge on functional features of natural DAases, as well as the knowledge driven from synthetic catalysts are the basis for the design of protein-based DAases. An efficient catalyst for DA reaction should therefore address the following points: *(i)* provide a cavity to place the diene and the dienophile in favorable positions to induce selectivity *(ii)* stabilize the TS of the desired coupling reaction and thus lower the activation energy. In this context, one key parameter to evaluate the efficiency of a catalyst is the rate acceleration or effective molarity (EM)[ii] that compares the rates of the catalyzed *vs*. uncatalyzed reactions under the same experimental conditions. In this review, we will present the different strategies that have been developed by researchers to prepare artificial enzymes for DA cycloaddition ranging from catalytic antibodies, computationally designed protein and artificial metallo-enzymes. An example of artificial enzyme for DA catalysis *in cellulo* will also be discussed.

[i] LepI is a counter-example. Although it acts as a matrix in positioning the substrates, its large and flexible binding pocket accommodates an ambimodal TS for both hetero-DA and homo-DA intramolecular cyclizations

[ii] Effective Molarity is the ratio between the first-order rate constant k_{cat} (min^{-1}) and the second-order rate constant k_{uncat} ($M^{-1}.min^{-1}$) determined for the uncatalyzed bimolecular DA reaction. It is also called “rate acceleration” in some articles

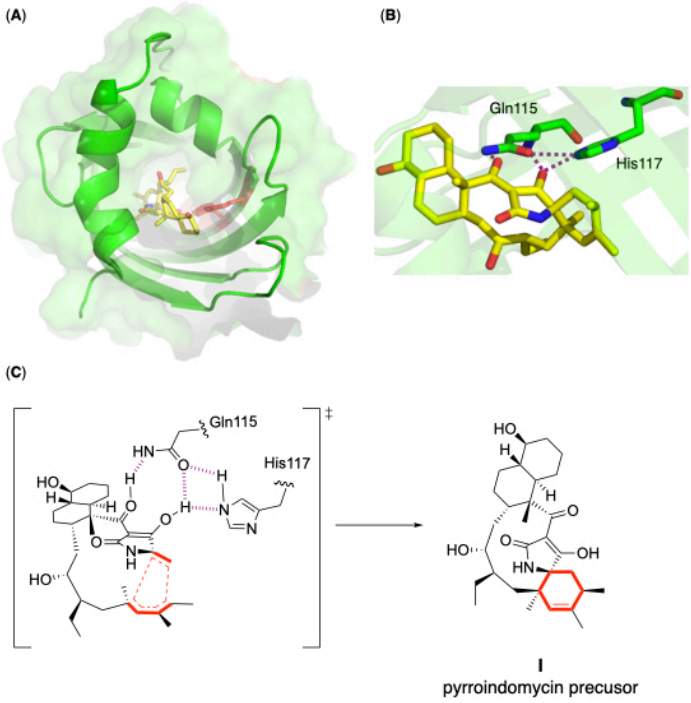

Figure 3. Structures of Pyrl4 (pdb: 5bu3)[47] in complex with the product spirotetramates pyrroindomycins **p**recursor **(I)**; (**A**) Ribbon diagram showing the hydrophobic cavity where **I** is bound (in yellow) and the Gln115 and His117 residues (in red); (**B**) Details of the H-bond network between **I** and Gln115 and His117 residues that inform on (**C**) the structure of the DA TS leading to **I**.

2. DA reactions catalyzed by antibodies.

2.1. Strategy and main achievements

Catalytic antibodies are antibodies selected to enhance the rate of a given reaction by binding its transition state. Using mammalian immune systems, several groups have successfully generated specific antibodies for DA reaction catalysis. The general strategy involves the generation of monoclonal antibodies selected to bind a hapten molecule that mimics the TS of the reaction (Figure 4).[50]

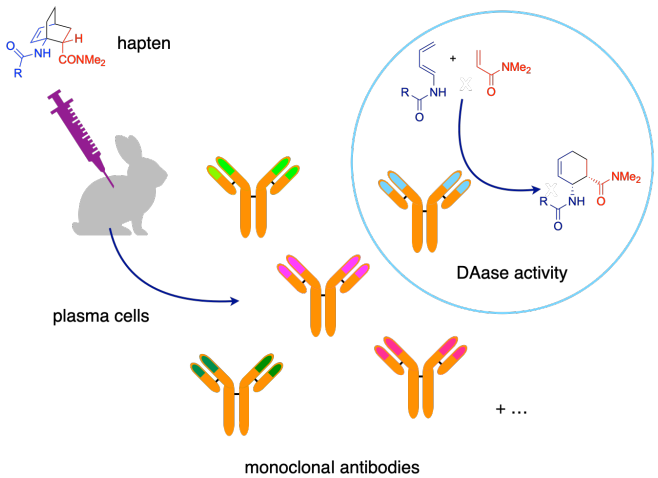

Figure 4. Strategy used for the generation of catalytic monoclonal antibodies.

The first catalytic antibody for a DA reaction was reported in 1989 by Hilvert *et al*.[51] This antibody (**1E9**) was elicited against the *endo*-hexachloronorbornene derivative **1**, a stable analog of the high-energy TS for the cycloaddition of tetrachlorothiophene dioxide and *N*-ethylmaleimide (Figure 5). **1E9** turned out to catalyze the DA reaction with a k_{cat} of 13 min^{-1} and EM of 10^3 M. The DA product spontaneously loses SO_2 leading to a product that does not resemble hapten **1**, thus avoiding product inhibition. The 3D structure of the **1E9** Fab fragment in complex with one hapten molecule was resolved at 1.9 Å resolution. It revealed that the antibody binding pocket provides significant shape complementarity with the hapten through Van der Waals contacts, π-stacking between TrpH50 residue and the maleimide moiety, and a H-bond between a carbonyl group from the maleimide moiety and AsnH35.[52] The good catalytic capability was explained by this high degree of shape complementarity between **1E9** and the transition state, as supported by quantum mechanical calculations.[53]

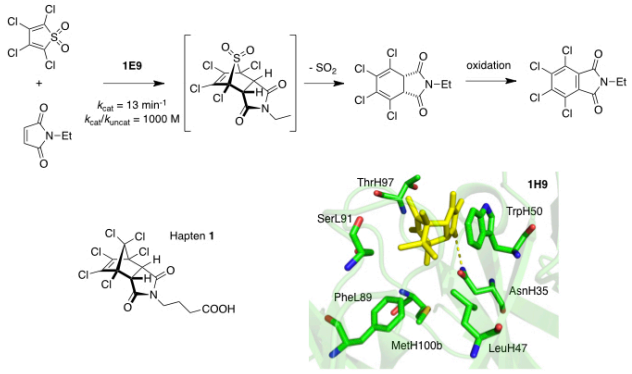

Figure 5. DA reaction catalyzed by the antibody **1E9** raised against *endo*-hexachloro-norbornene **1** and X-ray structure of antibody **1E9** including the hapten **1** (pdb: 1c1e).[52] H and L-labels of amino acid residues refer to the heavy and light chains of antibody, respectively.

The group of P. Schultz then reported on the generation of antibodies raised against bicyclo[2.2.2]octane hapten **2**, designed as a mimic of the boat-like transition state of the DA cycloaddition of the corresponding diene and dienophile (Figure 6). One among 10 antibodies specific for hapten **2, 39-A11** was found to catalyze the formation of the *endo* product with a k_{cat} of 40 min^{-1}.[54] The Fab fragment of **39-A11** was overexpressed,[55] and its X-ray crystallographic data in complex with hapten **2** were reported.[56] It revealed that the antibody binds the substrates in a reactive conformation presumably reducing translational and rotational degrees of freedom. The mechanism of stereoselective binding of enantiomeric haptens by antibody **39-A11** was studied by Zhang *et al*. using docking simulations and quantum mechanical models.[57] Based on these data, the stereoselectivity of **39-A11** was associated to a strategically-positioned H-bond with AsnH35 and π-stacking of the maleimide with TrpH50 at the antibody binding site (Figure 6).

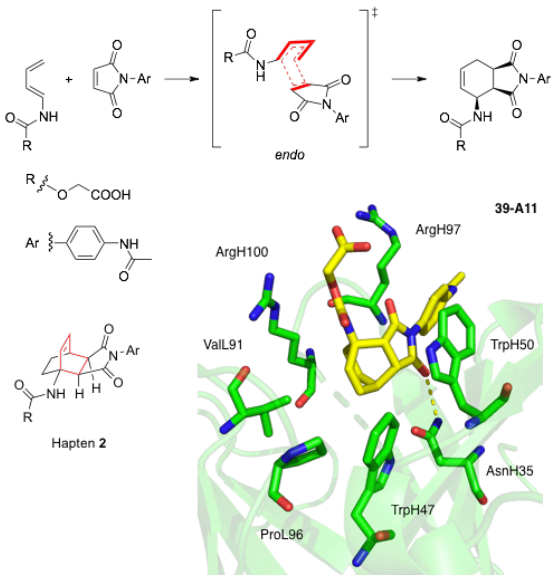

Figure 6. DA reaction catalyzed by antibody **39-A11** raised against the bicyclic hapten **2** and X-ray structure of antibody **39-A11** including the hapten **2** (pdb: 202w). H and L-labels of amino acid residues refer to the heavy and light chains of antibody, respectively.

After these first examples, several groups have employed a similar strategy and provided antibodies to catalyze homo-DA, [58,59] hetero-DA[60,61] as well as aza-DA[62,63] cycloadditions.

Among all these examples, one should mention the antibodies developed to catalyze the DA reaction of *trans*-1-*N*-acylamino-1,3-butadiene and *N,N*-dimethylacrylamide leading to the adduct **3** (Figure 7), a reaction that was used as model for computationally designing DAases (see section 3). Antibodies were generated using two strategies.[58,59]

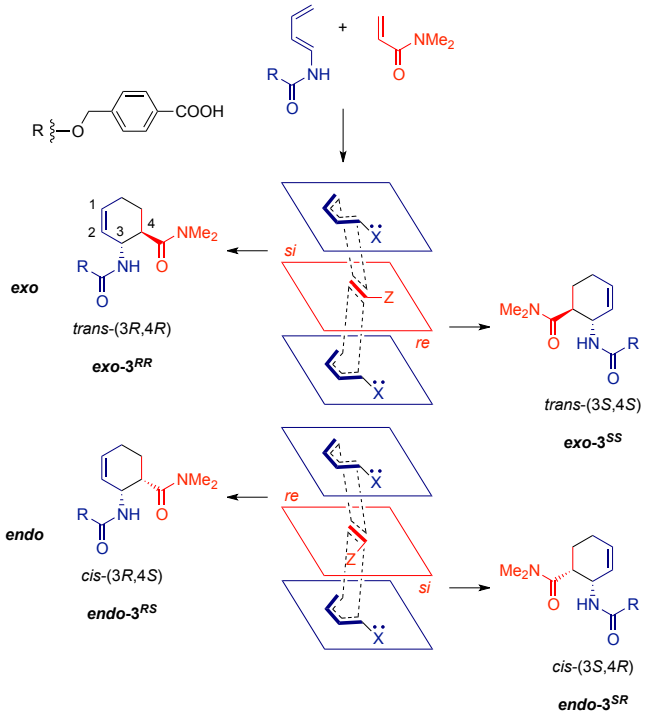

Figure 7. Diastereo- and enantioselectivities in DA reaction of 4-carboxybenzyl *trans*-1,3-butadiene-1-carbamate and *N,N'*-dimethylacrylamide (Ẍ = NHCOR and Z = $CONMe_2$)

Table 1. Kinetic parameters and stereoselectivity observed for the DA reaction of 4-carboxybenzyl trans-1,3-butadiene-1-carbamate and *N,N'*-dimethyl-acrylamide catalyzed by monoclonal antibodies (mAb) (entries 1-4) and *de novo* designed enzymes (entries 5-10).

Entry	Catalyst	*endo*:*exo* [*ee* (%)]	k_{cat} x 10^3 (min^{-1})	CE* ($M^{-2}.min^{-1}$) [$M^{-2}.s^{-1}$]	EM† (M^{-1})	Ref.
1	mAb **7D4** (**4**)	Complete *endo* [***endo-3^{RS}*** > 98%]	3.44	2108 [35]	48	[58]
2	mAb **22C8** (**5**)	Complete *exo* [***exo-3^{SS}*** > 98%]	3.17	604 [10]	18	
3	mAb **13G5** (**6**)	*exo* > 98% [***exo-3^{SS}*** > 95%]	1.2	-	6.9	[59]
4	mAb **4D5** (**7**)	*endo* > 98% [***endo-3^{RS}*** > 95%]	3.48	-	4.9	
5	**DA_20_00**	Complete *endo* [***endo-3^{RS}*** > 99%]	1.66	3.6 [0.06]	4	[64]
6	**DA_20_10**		35	366 [6]	94	
7	**DA_20_20**		75	2 040 [34]	199	[65]
8	**CE6**		36.7	5 220 [87]	97	[66]
9	**CE11**		73.3	3 000 [50]	194	[65]
10	**CE20**		180	32 400 [540]	478	

* Catalytic Efficiency, $k_{cat}/K_{Mdiene}.K_{Mdienophile}$.† Effective Molarity is the ratio between the first-order rate constant k_{cat} and the second-order rate constant k_{uncat} (7.15 and 1.75 10^{-4} $M^{-1}min^{-1}$ for the *endo* and *exo* adducts, respectively).

The first one reported by Gouverneur *et al.* involved the generation of monoclonal antibodies raised against two diastereoisomers of rigid bicyclic hapten used as transition state analogs for this reaction (**4** and **5** in Figure 8A).[58] One antibody, **7D4**, raised against hapten **4** catalyzed the favored *endo* reaction and the other, **22C8**, raised against hapten **5**, catalyzed the disfavored *exo* pathway to yield the respective *cis* and *trans* adducts in enantiomerically pure forms with respective k_{cat} of 3.17 x 10^{-3} and 3.44 x 10^{-3} min^{-1} (Table 1, entries 1 and 2). X-ray structures of the haptens were compared with the calculated transition state structures showing that **4** and **5** are excellent mimics of the transition states of the DA reactions. One main achievement in this study is the generation of a Diels-Alder catalyst for the kinetically disfavored process. In the particular case of the underprivileged *exo* process, it has been suggested that the binding energy must be used to redirect the reaction along the higher energy pathway. The energy requirements for the control of the stereochemistry in DA reactions is generally around 20 kcal/mol, which can be easily delivered by substrates binding to the antibody.

In another original approach to produce DAase antibodies that could catalyze the formation of either *exo*- or *endo*-cycloadducts, Janda and co-workers have employed ferrocenyl haptens **6** and **7**.[59] These flexible haptens, with cyclopentadienyl rings able to rotate freely in solution, were designed assuming that the immune system could freeze out a conformer which mimics the DA TS. Antibody **4D5** raised against hapten **7** catalyzed the favored endo-cycloaddition with k_{cat} of 3.48 x 10^{-3} min^{-1} with an EM close to 5 M (Table 1, entry 4). Antibody **13G5**, raised against **6**, was found to catalyze the disfavored *exo*-cycloaddition reaction between the corresponding diene and dienophile (Figure 8B) in high diastereo-selectivity with a k_{cat} of 1.2x10^{-3} min^{-1} with an EM close to 7 M (Table 1, entry 3). The crystal structure of the **13G5** Fab complexed to the acidic form of hapten **6** was determined.[67] It revealed a ferrocene moiety completely buried in the antibody with the ring rotation restricted by steric restraints imposed by specific hydrogen-bonding with the antibody binding pocket. Cannizzaro *et al.* synthesized the enantiomerically pure DA adduct using **13G5** as well as other monoclonal antibodies from the same immunization process.[68]

Quantum mechanics calculations were then used to rationalize the effects of different catalytic residues on the transition states resulting in the observed enantioselectivity of the DA reaction catalyzed by **13G5**. Their studies suggested that the hapten **6** used for screening antibodies bears a close resemblance to the Van der Waals complex of the reactants.

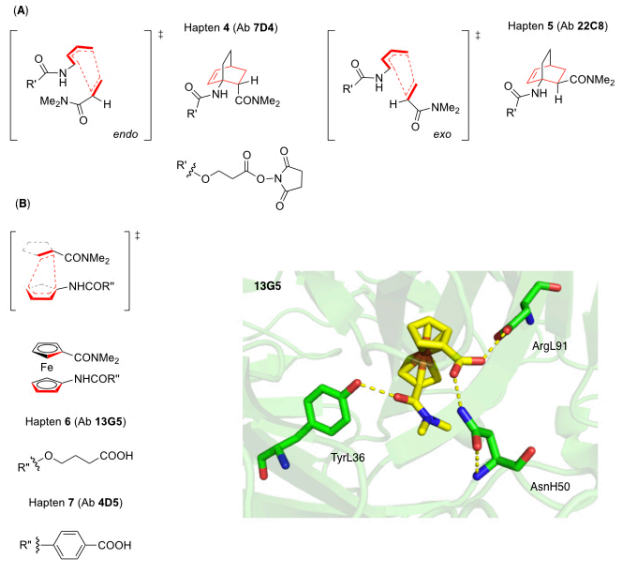

Figure 8. DA reaction of 4-carboxybenzyl *trans*-1,3-butadiene-1-carbamate and *N*,*N*'-dimethylacrylamide catalyzed (A) by antibodies **22C8** and **7D4** raised against the bicyclic haptens **4** and **5**; (B) by antibodies **13G5** and **4D5** raised against ferrocenyl haptens **6** and **7**. RX structure of the **13G5** with the 1-carboxy-1'-[(dimethylamino)carbonyl] inhibitor (pdb: 1a3l).

2.2. Conclusion and perspectives

Despite the prospects offered by the catalytic antibodies in DA reactions, this approach was rapidly abandoned in favour of computational design and artificial metalloenzymes (*vide infra*). One drawback of this strategy is that it is limited to one scaffold. In addition, both the difficult synthetic availability of the hapten molecules and the production of specific monoclonal antibodies by mammalian immunization appear as severe limitations to the development of antibody-based DAases. However, this approach could become attractive again in the light of recent progresses in the production of monoclonal antibodies by phage display technology therefore by-passing the long process of immunization and offering the possibility to further evolve better catalysts.[69]

3. DA reactions catalyzed by computationally designed enzymes

3.1. *De novo* design of a Diels-Alderase

Computational enzyme design has made substantial progresses in recent years following the development of tools for accurate protein structure modeling, prediction of protein stability and prediction of protein-ligand interactions.[70-74] Computational design strategy starts with the generation of a minimal active-site geometry containing selected protein residues to stabilize the computed TS for the desired reaction through non-covalent interactions (so-called theozyme). A protein that adapts to the TS and provides a protection from the outer-medium is then computationally selected,[75-80] and can be further optimized. Computational enzyme design therefore shares similarities with the catalytic antibody technology although a computationally generated TS is used instead of a synthetic hapten to select a protein template.

Siegel and coworkers have reported on the only example of *de novo* computationally designed DAase.[64] They chose the DA reaction of 4-carboxybenzyl *trans*-1,3-butadiene-1-carbamate and *N*,*N*'-dimethylacrylamide to generate the ***endo*-3^{RS}** enantiomer, a model reaction that had previously been targeted using antibodies (Figure 9).

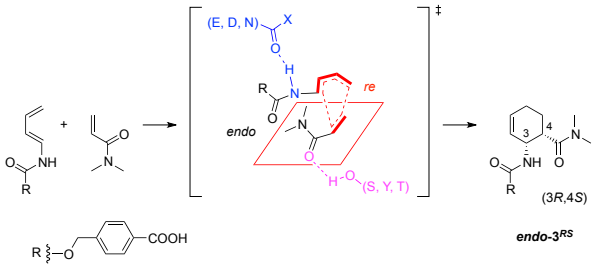

Figure 9. DA reaction of 4-carboxybenzyl trans-1,3-butadiene-1-carbamate and *N*,*N*'-dimethylacrylamide.

Computational design started with DFT calculations of the lowest energy TS (leading to the desired ***endo*-3^{RS}** product) in presence of several amino acid residues explicitly included as functional groups to activate the diene and dienophile (a glutamine or an asparagine to hydrogen bond with the N-H of the diene carbamate and a serine, threonine or tyrosine to hydrogen bond with the carbonyl oxygen of the amide of the dienophile). Starting from these structures, a set of conformers was generated by varying the rotameric states of the substrates, the amino acid residues and the hydrogen bonds geometries. The resulting set composed the so-called "theozymes" that represent minimal active sites for the desired reaction. These theozymes were then confronted to a bank of 207 structurally characterized proteins from the Protein Data Bank (pdb) using the RosettaMatch program.[80,81] The strategy is schematized in Figure 10.

The matches were then further optimized to generate mutations and optimize interactions between ligands and the host proteins. 84 designs were selected, the corresponding proteins were expressed in *E. coli* and only two were found to be able to catalyze the desired DA reaction: **DA_20_00** and **DA_42_00**. In both cases, one glutamine and one tyrosine composed the catalytic amino acids. X-Ray crystallography data obtained for one active variant of **DA_20_00** confirmed the good match between the structure and the design. The catalytic performances of the best designed enzyme, **DA_20_00**, were however modest with k_{cat} of 1.66 x10^{-3} min^{-1} and an EM = 4 M (Table 1, entry 5). Directed mutagenesis experiments of active site residues were performed to generate enzymes with improved catalytic efficiencies. **DA_20_10** was the most efficient with k_{cat} = 35 x10^{-3} min^{-1} and a rate acceleration of 94 M (table 1, entry 6). It turned out to be both highly stereoselective and substrate-specific - even small changes on the substrates led to drastic loss of activity, consistent with the active site being adapted to the substrates.

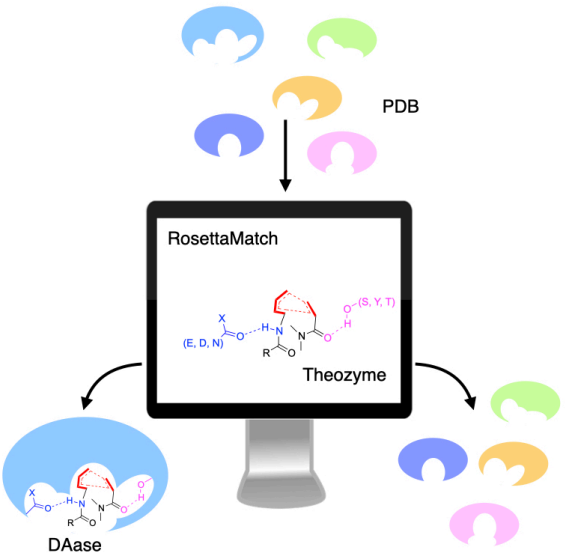

Figure 10. Strategy used to computationally design a DAase.

3.2. Biocatalysts improvements

Although, successful computational design of an enzyme catalyzing an enantio- and diastereoselective intermolecular DA reaction was achieved, the catalytic performances remained modest and different strategies were employed to improve the biocatalyst.

Firstly, Eiben *et. al.* reported on a game-driven strategy to improve the **DA_20_10** enzyme.[66] The online game Foldit is a crowdsourcing computer game centered on protein folding and allowing protein structure prediction and protein design.[82] Foldit players were asked to remodel some active site loops to have the substrates less exposed to solvent. In the first place, players were allowed to delete or insert up to 5 residues of any of the loops to create additional contacts with the ligands, as well as to mutate residues in the active site. The resulting *ca*. 70 000 designs were ranked in energy and the lowest-energy designs were visualized. Based on favorable interactions with the ligands, four designs were selected to undergo further improvements by "advanced players". The latter designed a library of 36 sequences starting from the 4 initial ones that provided better substrates stabilization. The enzymes were expressed and disappointedly, only one variant (named **CE0**) displayed very low activity, probably due to non-optimal interactions with the substrates. 500 additional sequences were then generated and evaluated, and this led to **CE4** variant that displayed a 10-fold improved catalytic efficiency (CE)[iii] as compared to the starting sequence (CE = 42 $M^{-2}.s^{-1}$), attributed to the presence of a helix-containing lid. The helix was followed by an unstructured loop and the Foldit players were asked, in a second round, to transform this unstructured loop into a structured helix. The most active design from this library, **CE6**, contained a 24-residue helix forming a lid interacting with the substrate. It resulted in an enzyme with significantly improved catalytic efficiency (87 $M^{-2}.s^{-1}$) with k_{cat} = 36.7 x 10^{-3} min^{-1} and EM = 97 M (Table 1, entry 8). The Foldit players were finally challenged to predict the structure of the lid and X-ray crystallography showed that the lid adopted a helix-turn-helix structure as predicted in the lowest-energy solution proposed by the Foldit players. Therefore, after several iterations of design and characterization, an

[iii] The Catalytic Efficiency (CE) = $k_{cat}/K_{Mdiene}.K_{Mdienophile}$ is expressed in $M^{-2}.s^{-1}$

enzyme was obtained displaying an 18-fold increased catalytic efficiency as compared to the original **DA_20_10** template associated with the addition of a lid providing better stabilization of the substrates in the active site.

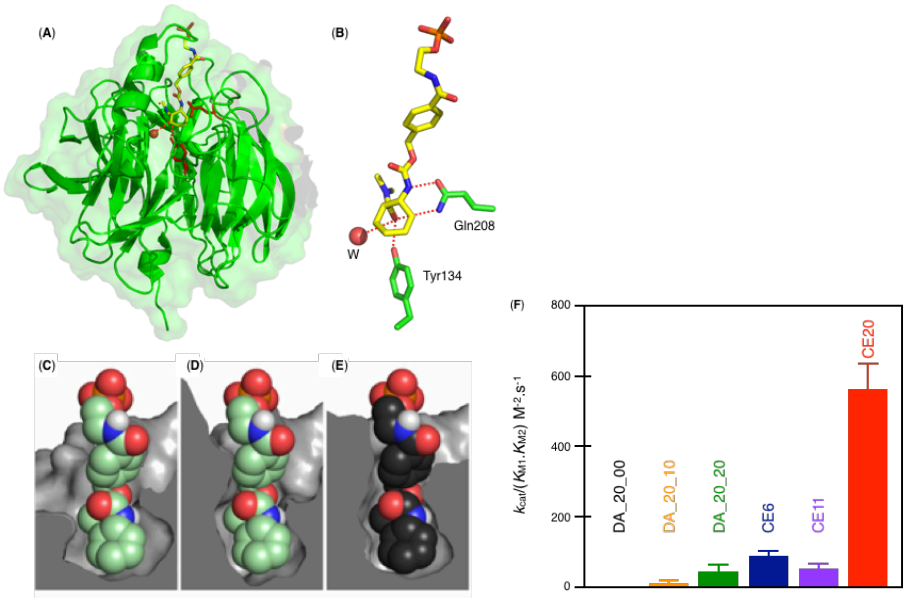

Figure 11. (*Top*). (**A**) Crystal structure of **CE20** (pdb: 4o5t) with bound product (**B**) Details of the catalytic residues Tyr314 and Gln208 and a buried water molecule that interact with the substrate. (*Middle*) Figure reproduced from Preiswerk *et al.*[65] Evolution of the active sites of **DA_20_00** variants (**C**) **DA_20_00** (one active variant) (**D**) **CE6**, and (**E**) **CE20**. The ligands in **DA_20_00** and **CE6** pockets (green carbons) were placed manually in the same orientation as the product seen in the crystal structure of the **CE20** complex (black carbons). (*bottom*) (**F**) Evolution of the catalytic efficiencies of **DA_20_00** and evolved variants. K_{M1} and K_{M2} are the Michaelis constants for the diene and the dienophile and k_{cat} is the first-order catalytic rate constant.

Secondly, Preiswerk *et. al.* have then performed several rounds of directed evolution by error-prone PCR (ePCR) to improve the DAase.[65] They started using **DA_20_10** as template and screened the resulting library for the most active variants. The best variant **DA_20_20** accumulated 5 surface-located mutations and 2 mutations in the hydrophobic core, remote from the active site. It catalyzed the DA reaction with k_{cat} = 75 x 10^{-3} min^{-1}, CE = 34 $M^{-2}.s^{-1}$ and CE = 199 M (Table 1, entry 7). To further improve the biocatalyst, the same mutations were generated on the **CE6** variant arising from the game-driven strategy, but the resulting variant (**CE11**) displayed catalytic performances not better than that of **DA_20_20** (Table 1, entry 9). **CE11** was thus subjected to further directed evolution by ePCR and after 8 rounds, the best variant (**CE20**) displayed significantly improved catalytic parameters (k_{cat} = 180x10^{-3} min^{-1}, CE = 540 $M^{-2}.s^{-1}$ and EM = 478 M) (Table 1, entry 10) which enabled preparative-scale synthesis of up to 30 mg of the ***endo*-3^{RS}** product in aqueous buffer and at room temperature with more than 90% conversion. The X-ray structure was solved in the presence of a substrate's analog and provided interesting insight into the structural basis for the evolutionary improvements (Figure 11). Although the catalytic residues and the shape of the active site were successfully designed in the initial theozymes, the first **DA_20_00** enzyme had a very opened active site in which the substrates were not tightly bound. Insertion of a lid (**CE6**) and further improvements of this lid and of the active site led to an enzyme (**CE20**) displaying a deep hydrophobic pocket in which the substrates are perfectly accommodated. The side chains of the catalytic tyrosine (Tyr134) and glutamine (Gln208) residues adopt similar positions in all structures (Figure 11A-B). It is noteworthy to mention that **CE20** does not suffer product inhibition.

3.3. conclusion and perspectives

CE20, derived from computational design after two optimization strategies, appears as one of the most selective and efficient artificial catalyst for DA reaction reported to date.[65] Indeed, the catalytic efficiency and the EM are *ca*. 15-fold and 10-fold higher respectively than that of **7D4**, the best catalytic antibody reported for the same reaction (Table 1). Interestingly, **CE20** is approaching the performance of natural DAases. Indeed, the CE of **CE20** (540 $M^{-2}s^{-1}$) is comparable to that of MaDA (120 $M^{-2}s^{-1}$), the unique intermolecular DAase,[42] supporting the fact that **CE20** behaves as an *entropy gap* that binds the substrates into a pocket containing residues that maintain/activate them in a conformation close to the one of the TS. This nice achievement is the result of several optimization rounds, highlighting the importance of evolution techniques in the design of efficient biocatalysts. Progresses in computational methods, together with the increasing protein scaffold libraries suggest that this strategy may be a promising one in the future to generate bio-catalysts for virtually any chemical reaction.[74,83,84]

4. DA reactions catalyzed by artificial metalloenzymes

4.1. General strategy

To our knowledge, natural metal-containing DAases have not yet been reported. While magnesium(II)-containing macrophomate synthase was initially thought to be a metallo-DAase,[85,86] it was later shown to more accurately catalyze a sequential Michael-aldol addition.[85,86] Nevertheless, the early mechanistic assumptions of dienophile bidentate coordination on magnesium(II) certainly played a role in inspiring the preparation of artificial metallo-DAases. The vast majority of these were designed for the DA cycloaddition of 2-azachalcones (**8a-f**) and cyclopentadiene (CP) (Figure 12). The catalysis was shown to proceed *via* the bidentate coordination of dienophiles **8a-f** on the metal center by the nitrogen and the oxygen of the pyridine and carbonyl group, respectively, making them more electron-deficient due to the Lewis acidity of the metal and thus more reactive (Figure 2).[17]

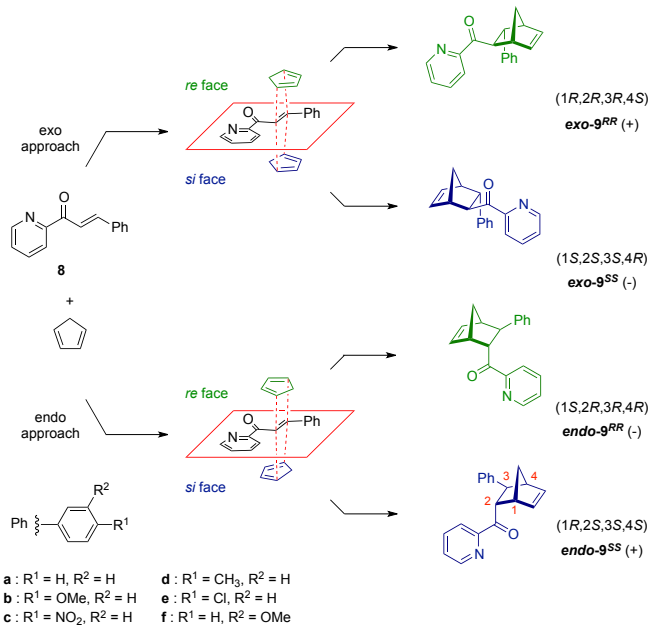

Figure 12. Diastereo- and enantioselectivities in DA reaction of 2-azachalcons (**8a-f**) and cyclopentadiene (CP).

Secondary orbital effects favor the formation of the *endo* isomers of the products **(9a-f),** however because of their protein components and the hydrophobic and chiral environment, artificial metallo-DAases are able to accelerate

the reaction and shift the *endo:exo* ratio as well as the enantiomeric balance of the products. It has been demonstrated that copper(II) was the most efficient water-compatible transition metal for the Lewis acid catalysis of this cycloaddition[87-90] and therefore most artificial metallo-DAases have been prepared by incorporating Cu(II) or its complexes into proteins by following one of the three strategies usually employed for preparing artificial metalloenzymes, *i.e.* supramolecular insertion (Figure 13A), covalent anchoring (Figure 13B) or metal coordination (Figure 13C).[6]

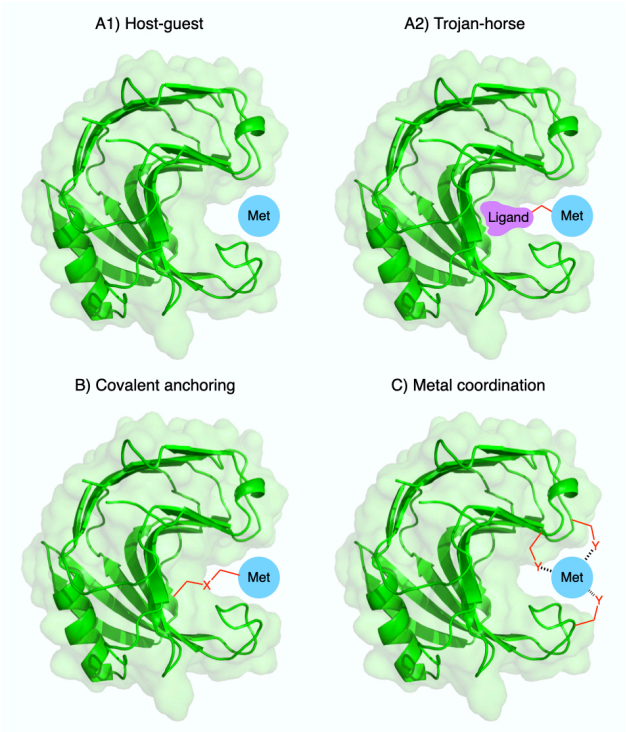

Figure 13. Strategies used to prepare artificial metallo-DAase.

4.1. Supramolecular insertion

The supramolecular insertion of metal cofactors into proteins can be achieved by following either the "host-guest strategy" or the "Trojan-horse strategy" (Figure 13). The former strategy relies on the inherent affinity of a protein for a metallic cofactor while the later relies on the covalent attachment of the metallic cofactor to an entity known to bind the host protein.

The first example of artificial metallo-DAase prepared following the host-guest strategy was reported by Reetz and coworkers (Figure 13A1).[91] Since albumins are carrier proteins known for binding metal complexes, different serum albumins were incubated with a water soluble copper(II)-phtalocyanine complex (**10**, Figure 14). The binding was evidenced by changes in the UV/Vis absorption spectrum of the complex upon addition of the protein, and further confirmed by MALDI mass spectrometry. In the case of bovine serum albumin based metallo-DAase (BSA⊂**10**) the products were obtained with 80% conversion with an *endo:exo* ratio of 96:4 and 93% *ee.* Although not discussed in the article a k_{obs} = 3.7 x 10^{-3} M^{-1} min^{-1} can be estimated from the data (Table 2, entry 1). The catalysis was then assayed using other sources of serum albumin and in particular using human and porcine serum albumins (HSA and PSA) and the obtained metalloproteins provided conversions reaching 89 and 87% respectively, but without improvement of neither the *endo:exo* ratio nor the *ee*. The BSA based DAase was subsequently employed for

screening the reaction with the other substrates (**8b-e**) and provided products with up to 91% conversion and 98% *ee* (substrate **8d**).

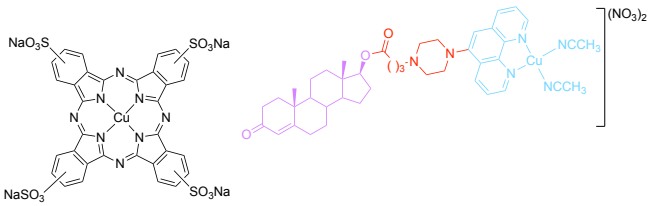

10 11

Figure 14. Copper(II) phtalocyanine complex **10** used in association with serum albumin and Trojan-horse **11** used with neocarzinostatin (catalytic center in blue, spacer in red and testosterone antagonist in violet)**.**

4.2. Covalent anchoring

This strategy relies on the reaction of an amino acid residue side-chain of the host protein, usually the thiol function of a cysteine residue (either already present or introduced by site-directed mutagenesis), with maleimide- or halogenoalkyl- containing ligands or complexes (Figure 13B). This strategy has frequently been employed and the different examples are summarized in Figure 15. A ligand (bipyridine, 1,10-phenanthroline, terpyridine etc) is generally covalently attached to the protein scaffold prior to the addition of a metal ion (copper in general). In few cases, direct anchoring of the prepared complexes was followed instead (Figure 15A and C **12** and **15a-c**).[94,107]

Table 2. Diastereo- and enantioselectivity parameters in DA reaction of 2-azachalcons **8a** and cyclopentadiene.

Entry	Catalyst	K_{cat} *or* k_{obs} [T°C]	Conv. (%)	*endo*:*exo*	*ee* (%)	Ref.
1	BSA⊂**10**	3.7 x 10^{-3} M^{-1} min^{-1},* [3°C]	80	96:4	93†	[91]
2	NCS-3.24⊂**11**	0.11 M^{-1} min^{-1},* [4°C]	83	81:19	no *ee*	[92]
3	SCP-2L_V83C-**13** SCP-2L_V83C-**14** SCP-2L_A100C-**13** SCP-2L_A100C-**14**	nd	19 87 43 76	88:12 93:7 92:8 95:5	25 (***endo*-9^{SS}**) 4 (***endo*-9^{SS}**) no *ee* 5 (***endo*-9^{RR}**)	[93]
4	FhuA-**15a** FhuA-**15b** FhuA-**15c**	nd	64 69 15	98:2 96:4 66:34	no *ee*	[94]
5	GTL_S114C-**16** GTL_S196C-**16**	nd	99 98	99:1 99:1	18 (***endo*-9^{RR}**) 92 (***endo*-9^{RR}**)	[95]
6	LmrR_M89C-**16** LmrR_M89C-**17**	nd	93 55	95:5 63:37	97 (***endo*-9^{SS}**) 66 (***endo*-9^{RR}**); 90 (exo)	[96]
7	A3_Y26C-**16** A3_F119C-**16**	nd	16 11	92:8 86:14	7.5 (***endo*-9^{RR}**) 62 (***endo*-9^{RR}**)	[97]
8	(A3_A3')_F119C-**16** (A3_A3')_F119C-**18**	nd	15 38	93:7 92:8	52 (***endo*-9^{RR}**) 5 (***endo*-9^{RR}**)	[98]
9	tHisFHHD	nd	73	93:7	46	[99]
10	$mTFP^{EHH}$ $mTFP^{CHH}$ $mTFP^{CHH}$ [pH = 6]	nd	99 89 97	92:8 94:6 93:7	15 <4 26 (***endo*-9^{SS}**)	[100]
11	bPP_Y7H bPP_Y7**19^{p}** bPP_Y7**19^{m}**	10.2 $M^{-1}min^{-1}$,* [5°C]	96 65 >99	95:5	3 6 83 (***endo*-9^{RR}**)	[101]
12	ACCO-Cu $Cu(NO_3)_2$ in buffer uncatalyzed	50 x 10^{-3} min^{-1} [4°C] - -	>99 50 5	99:1 82:18 82:18	95 (***endo*-9^{RR}**) no *ee* no *ee*	[102]
13	NB-**20**	nd	22	90:10	no *ee*	[103]
14	NB4-Pyr [(*R*) conf.] NB6-Pyr [(*S*) conf.]	nd	56 40	95:5 92:8	69 (***endo*-9^{SS}**)	[104]
15	A2A⊂**21**	nd	28	82:18	19 (***endo*-9^{RR}**)	[105]

All the reactions were performed in buffer containing Cu(II) salts except for FhuA-**15a-c** that were obtained directly by grafting the copper(II) complexes **15a-c**. * second order rate constant (k_{obs}) † Absolute configuration of the endo product was not provided.

Covalent anchoring in proteins with natural cavities

An artificial metallo-DAase was prepared using a (η^6-arene)-ruthenium(II) complex (**12**) and papain as protein template (Figure 15A).[107] In this case, the reactivity of the resulting artificial metalloenzyme was evaluated for the DA reaction of acrolein and CP. The protein environment indeed accelerated the reaction (at 0.2 mol % loading, k_{obs} = 14.6 x 10^{-3} min^{-1} and k_{cat}/k_{uncat} ~ 3 M) but no *ee* was detected in the products. This was explained by the fact that the cysteine residue that was employed for binding the complex was located at the entrance of the catalytic pocket at the protein surface. The anchored complex and substrates could interact with only a few amino acid residues leading to a poor control of the selectivity of the reaction. This work illustrates the importance of the protein scaffold as well as the complex anchoring position.

Several proteins scaffolds were then chosen (Figure 15). Among them, Nitrobindins (NB) [103] that will be described in another subsection (4.4). The following examples were carried out on the model reaction of the DA cycloaddition of 2-azachalcones (**8a-f**) and CP.

On example relies on the cylindrically-shaped hydrophobic cavity of the sterol carrier protein type 2 like domain (SCP-2L) of multifunctional enzyme type 2 (MFE-2) (Figure 15B) reported by Kamer *et al*.[93] The covalent anchoring of 1,10-phenanthroline (**13**) or dipicolylamine (**14**) carrying maleimide functional groups were performed on V83C and A100C variants. The hybrids provided rather modest catalytic performances for the DA reaction. In the best case, 25% *ee* in favor of the ***endo*-9^{SS}** product was obtained (Table 2, entry 3).

Another example was reported by the group of Okuda. [94] A variant of the relatively robust transmembrane protein, Ferric hydroxamate uptake protein component A (FhuA) was used to prepare an artificial metallo-DAase (Figure 15C).[94] Bioconjugation was achieved by the reaction of C545 of FhuA with different terpyridine copper(II) complexes with variable linkers between the maleimide group and the terpyridine (**15a-c**). The best result for DA reaction catalysis was obtained with the shorter linker, *e.g.* using **FhuA-15a** bio-conjugate (Table 2, entry 4). This was attributed to the lower flexibility of the metal complex within the β-barrel core of the protein. In all cases, no enantioselectivity was observed suggesting that there are no preferential orientations of the substrates within the cavity.

In an original approach, Palomo and coworkers generated a large amount of a heterogeneous artificial metalloenzyme (about 10 mg per g of support) by assembling the 1,10-phenanthroline-copper(II) complex (**16**) and sepabeads-bound *Geobacillus thermocatenulatus* lipase (GTL).[95] Firstly, site-directed mutagenesis was used to remove two native cysteine residues and introduce one cysteine residue either at the active site (S114C), or in a pocket expected to be well-suited to accommodate the substrates (S196C) according to molecular modelling results (Figure 15D). Secondly, the enzyme variants were overexpressed and purified by immobilization on sepabeads *via* either single covalent binding to the *N*-terminal (SB-NH_2) or multiple covalent binding to a lysine-rich region of the protein surface (SB-Lys). Finally, introduction of complex **16** led to immobilized artificial metalloenzymes. Catalysis was assayed for the DA cycloaddition of **8a** and CP. For both variants, immobilization through the lysine-rich region gave better results and in particular the artificial enzyme SB-lys-GTL296-**16** provided an *endo:exo* ratio of 93:7 and 92% *ee* (98% conversion) (Table 2, entry 5). These results were significantly enhanced as compared to the ones obtained with the soluble forms of the artificial enzymes. Docking experiments were conducted and led to the conclusion that, in the case of the cysteine in position 196, several protein residues were involved in the stabilization of the phenanthroline ring leading to a precise orientation of the attached Cu-complex towards the incoming substrates, thus rationalizing the excellent enantioselectivity observed in this case.

Covalent anchoring in proteins with cavities generated at dimeric interfaces

Another way to design artificial metallo-DAases takes advantages of hydrophobic pockets generated at dimeric protein interfaces. Two examples have been reported in the literature using this approach.

The group of Roelfes have used Lactococcal multidrug resistance regulator (LmrR) to generate copper-containing artificial metallo-DAases.[96] A cysteine residue was introduced by site directed mutagenesis to enable the binding of either 1,10-phenanthroline or 2,2'-bipyridine ligands carrying bromoacetamide functional groups (**16** and **17** in Figure 15E). Since LrmR dimerizes in solution, the mutation M89C was chosen in order to introduce two copper(II) complexes at the dimer interface and at a distance large enough to avoid complex-complex interaction. Each protein dimer thus provided two independent DA catalysts. (Figure 15E). After metalation with copper(II), the catalysis was assayed on the DA cycloaddition of either **8a**, **8e** or **8f** and CP and it resulted that the 1,10-phenanthroline based artificial enzyme (LmR_M89C-**16**) was the most efficient one. The best result of 93% conversion, 95:5 *endo:exo* ratio and 97% *ee* was obtained starting from substrate **8a** (Table 2, entry 6). Interestingly, LmrR_M89C-**17**, based on 2,2'-bipyridine, gave rise to 66 % *ee* of the opposite *endo* enantiomer, and therefore by changing the Cu(II) ligand, both enantiomers of the DA *endo* product could be accessed.

Finally, Di Meo *et al.* have reported on the generation of artificial enzymes, including DAases using A3αRep, a member of artificial protein family based on a thermostable α-helical repeated motif.[97] A3αRep forms a stable homo-dimer with a wide cleft in which two positions, one at the edge (Y26) and one in the center (F119) were changed independently into cysteine residues. Then, a phenanthroline ligand carrying bromoacetamide (**16**) was covalently attached to the cysteine of each protein variant (Figure 15F). The enzyme A3_Y26C-**16** therefore bears two ligands located at the edges of the cleft (C26) and can coordinate two copper(II) equivalents per dimer. The catalytic properties of A3_Y26C-**16**, were poor with low ee (Table 2, entry 7). On the other hand, the enzyme with the ligands in the center of the cleft (A3_F119C-**16**) led to an active site with mainly one copper(II) ion coordinated by the two phenanthroline ligands provided by the two independent monomers. This is in agreement with the low conversion observed in the catalytic assays, the copper(II) ion displaying a saturated coordination sphere and being unable to interact with substrate **8a**.

In order to improve the efficiency of the system, a chimeric enzyme formed by the native A3αRep domain and an A3αRep bearing a single cysteine (F119C) was generated.[98] After bioconjugation with phenanthroline and metalation by copper(II), (A3_A3')_F119C-**16** was shown to contain only one Cu(II) equivalent. However, although an increased conversion was obtained, the absence of the second phenanthroline provided a more opened cavity and the *ee* dropped to 5% (Table 2, entry 8). By using the bulkier terpyridine ligand (**18**), (A3_A3')_F119C-**18** displayed lesser conversion but an *ee* of 52 % .

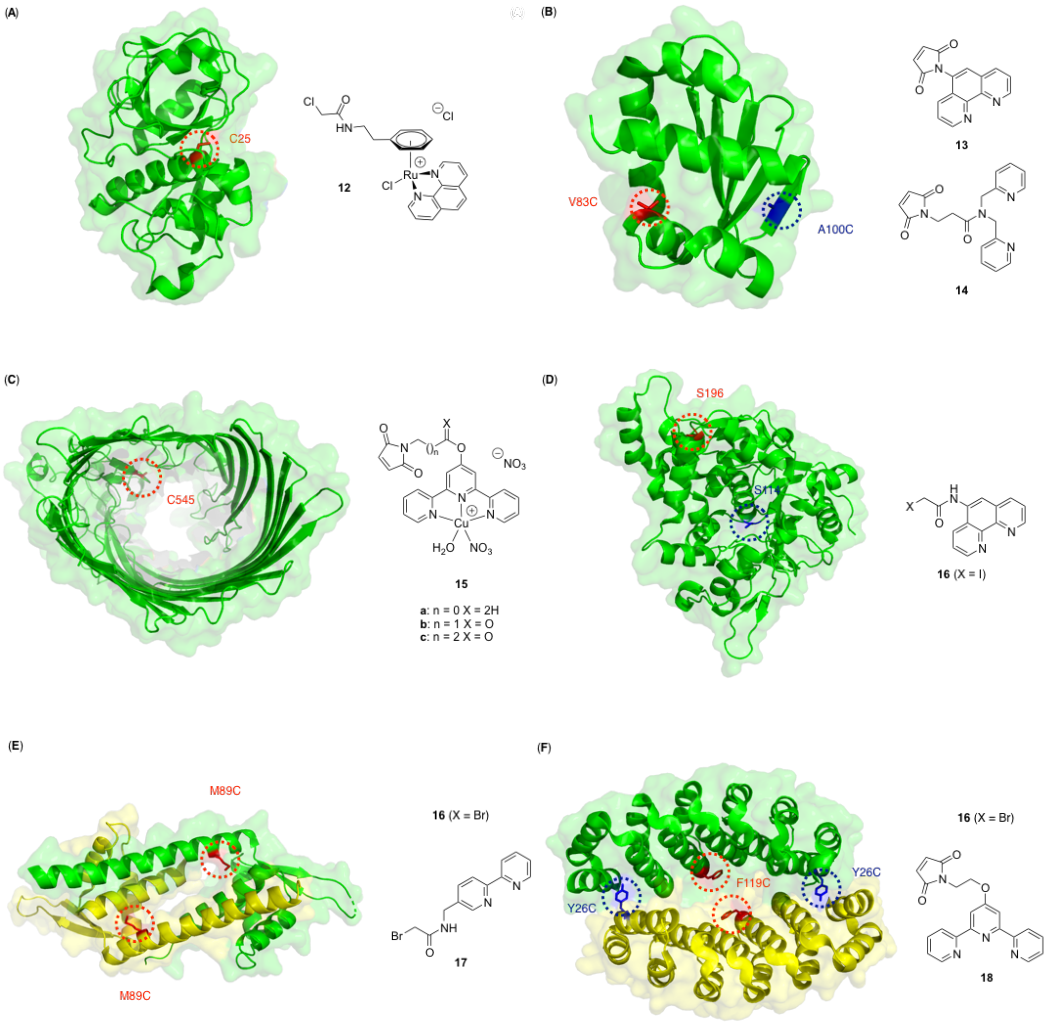

Figure 15. Protein scaffolds used in artificial DAases with on the left ligands or metal complexes that were grafted on the protein to the highlighted residues. (**A**) Papain (pdb: 6h8t) showing the C25 residue; (**B**) SCP-2L (pdb: 1ikt) showing the A100 (in blue) and V83 (in red) residues that were the subject of single point mutation into cysteine.; (**C**) Mutant protein FhuAΔCVF^{tev} (pdb: 2fcp) showing the residue C545; (**D**) *G. thermocatenulatus* lipase (pdb: 2w22) showing the S114 (in blue) and S196 (in red) residues that were the subject of single point mutation into cysteine; (**E**) LmrR dimer (pdb: 3f8f) showing the M89 residue that was the subject of single point mutation into cysteine; (**F**) A3αRep-A3αRep dimer (pdb: 3ltj) showing the Y26 (in blue) and F119 (in red) residues that were the subject of single point mutation into cysteine. The structures based on the crystallographic data were obtained using PyMol software.

4.3. Metal coordination

The last strategy to introduce a metal ion into a protein scaffold relies on the use of endogenous protein ligands *e.g.* either the active site of a metalloproteins (in its apo-form) or an artificial site generated by directed mutagenesis.

Metal coordination to an artificial binding site introduced by mutagenesis

Three examples were reported using this approach. The first one was described by Reetz and co-workers.[99] The thermostable synthase subunit of imidazole glycerol phosphate synthase (tHisF) from *Thermotoga maritima* was mutated to obtain a transition-metal binding site. Guided by nature, the group engineered a His/His/Asp binding site to accommodate a copper center. Additionally, all other histidine residues were mutated into alanine to avoid non-specific copper binding outside the engineered active site. Catalysis of the DA cycloaddition of **8a** and CP by the engineered enzyme resulted in up to 73% conversion, *endo:exo* ratio of 93:7 and 46% *ee* (Table 2, entry 9).[99] By following a similar approach, *Fischer et al.* have used a monomeric, pH- and thermo-stable version of *Clavularia* cyan fluorescent protein (mTFP1).[100] Mutagenesis experiments were first performed to remove native histidine and methionine residues and delete flexible *N*- and *C*-terminal sequences. Mutants I197C−Y200H−Y204H (mTFP^{CHH}) and I197E−Y200H−Y204H (mTFP^{EHH}) were generated and the copper-containing proteins were used to catalyze the cycloaddition of **8a** and CP at pH ranging from 3.5 to 7.5. Both enzymes gave low enantio and regio selectivities. Additional mutations were introduced to mTFP^{CHH} at the edge of the metal binding cavity. These changes within the second coordination sphere led to an increase of ee from <4 to 26 % at pH6 (Table 2, entry 10)

A third example was obtained using Bovine pancreatic polypeptide (bPP), a small hormone of thirty six amino acids that adopts a dimeric structure in solution (Figure 16).[108] After truncation of residues 31 to 36 that induce a disorder in the structuration of bPP, amino acid ligands for copper(II) binding were introduced.[101] Based on molecular modeling,[109] Tyr7 was replaced by amino acids such as histidine, or the non-proteinogenic 3- and 4-pyridylalanine (**19*m*** and **19*p***). The position 7 is located at the dimer interface and at a distance of the other subunit that allows coordination of both residues to the metal ion. Using bPP_Y7H and bPP_Y7**19*p*** variants, the cycloadducts were obtained with very low *ee* (Table 2, entry 11). On the contrary, with quantitative yield, an *endo:exo* ratio of 95:5 and 83% *ee*, bPP_Y7**19*m*** variant proved to be a highly functional DAase (Table 2, entry 11). However, the Y7X mutation led to a drastic decrease in dimerization affinity and in the catalytic conditions, the catalyst was predominantly found in a monomeric form. In these conditions, since copper(II) binding to a single pyridine is weak, it was proposed that, in addition to **19*m*,** other residues in the peptide are likely involved in the binding of the Cu(II) ion**.**

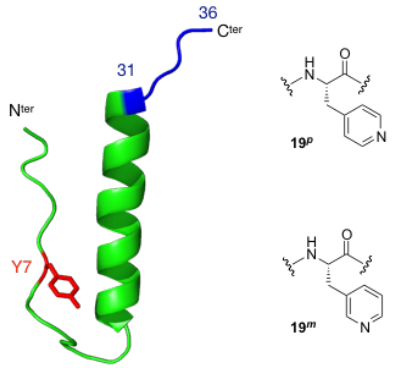

Figure 16. NMR structure of the bPP (pdb: 1bbA) showing the α-helix scaffold with the truncated residues (in blue) and the Y7 residue (in red) that is replaced by His and non-proteinogenic amino acids **19*p*** and **19*m***.

Metal coordination to endogenous amino-acids

Ghattas *et al.* have reported on metal-substitution at the active site of an iron-containing metalloenzyme to generate a DAase.[102] Copper(II) was added to *apo*-1-aminocyclopropane carboxylic acid oxidase (ACCO) instead of the native iron(II).[110] The copper(II)-reconstituted enzyme (ACCO-Cu) was used to catalyze the DA cycloaddition of **8a-c** and CP and provided up to quantitative yield and >99 % *ee* in favor of the ***endo*-9a^{RR}** product (Table 2, entry 12). This unprecedented performance was rationalized by molecular modeling, which suggested that only one coordination geometry of **8a** in the active site was possible and that only one path was accessible for CP to react with the bound **8a**, thus limiting the number of possible product isomers from four to one (Figure 17).

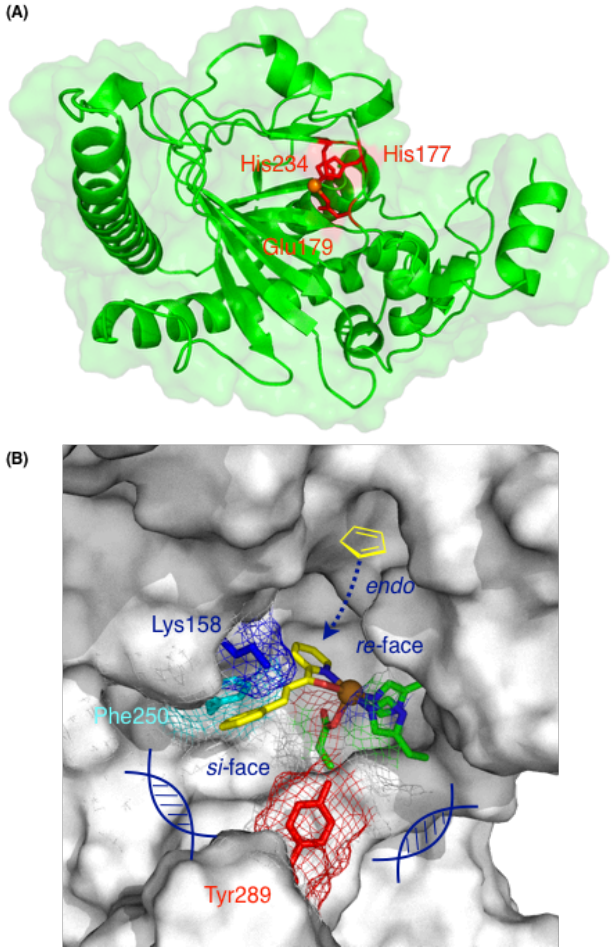

Figure 17. (**A**) Crystal structure of ACC oxidase (pdb: 1w9y) showing the protein structure with the His177, Glu179 and His234 residues (in red) involved in the complexation of the Cu(II) ion (orange sphere). (**B**) Docking experiments results showing substrate **8a** as a stick model in the active site of ACCO-Cu(II) and the CP approach.

4.4. Mixed approaches

The group of Hayashi has developed a mixed approach between covalent and supramolecular to generate artificial metallo DAases using Nitrobindins (NB) as scaffold (Figure 18). NBs belong to an ubiquitous family of all β-barrel proteins that display hydrophobic cavities containing a labile native heme cofactor.[111] Several NB variants were prepared. All of them contained a cysteine residue in position 96 (C96, Figure 18). In a first place, following a classical “covalent anchoring approach” a terpyridine ligand **18** was covalently attached to the cysteine C96.[103] In the presence of Cu(II) salts, NB4-**17** catalyzed the DA reaction of **8a** and CP with modest performances. While the

endo:exo ratio was relatively high (90:10), the conversion was low (22%) and no *ee* was observed (Table 2, entry 13). The results were not improved when Zn(II) or Co(II) were used in place of Cu(II).

In order to improve the performance of the catalyst, a different approach was used.[104] To reduce the space inside the cavity of NB, *N*-(1-pyrenyl)maleimide (**20**) was grafted on C96. Interestingly, the stereoselectivity of the grafting reaction was governed by the different environments provided by the protein variants (NB1-6). Pyrene was thus bound into the NB cavities either in the (*R*)-conformation or the (*S*)-conformation, depending on the NB variant (Figure 18). They subsequently demonstrated that the modified proteins had an affinity for **8a** due to aromatic interactions with the pyrene moiety. Addition of CP and copper(II) salt to the preorganized NB-Pyr⊂**8a** led to the formation of DA adduct. The NB4-Pyr variant for which the (*R*)-conformation was favored led to the best results with a 56% conversion, *endo:exo* ratio of 94:6 and 69% *ee*. While the NB6-Pyr variant for which the (*S*)-conformation was favored led to rather modest performances (Table 2, entry 14).

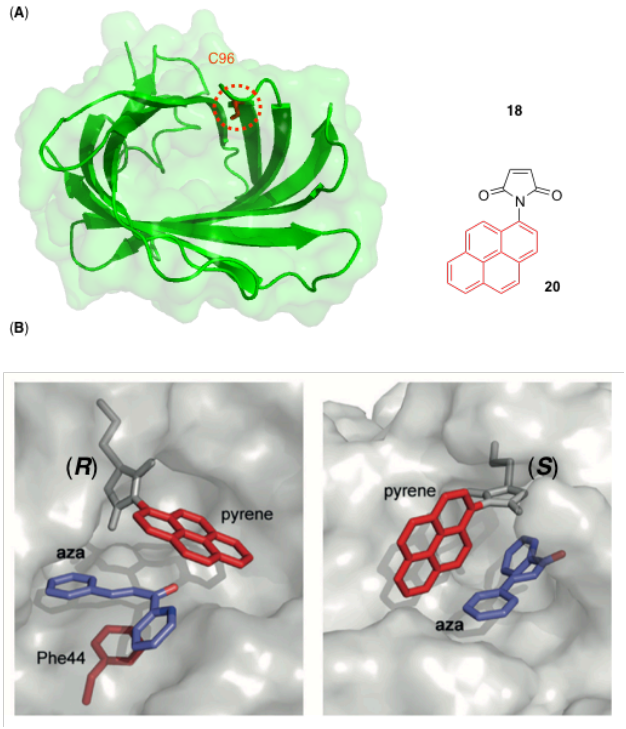

Figure 18. Crystal structure of the Nitrobindin protein (pdb: 3wjb) showing (**A**) the β-barrel protein scaffold with the C96 residue (in red) on which pyrene **20** or terpyridine **18** derivative are grafted and (**B**) the energy minimized structures of NB4-Pyr in (*R*)-configuration carbon and (*S*)-configuration carbon with **8a** (aza in purple). Figure reproduced from Himiyama *et al.*[104]

4.5. Towards *in cellulo* biocatalysis of DA reaction

Although significant efforts are directed towards the development of *in vivo* or *in cell* biocatalysis,[7-10] there is only one example of artificial enzyme for *in vivo* DA catalysis reported in the literature.[105] One problem faced by *in vivo* catalysis employing transition metal complexes is the potential deactivation inside the living cell due to the large amounts of possible inhibitors such as glutathione, in particular in the case of Cu(II) ion.[112] One way to protect catalysts is their tight incorporation into a protein scaffold and/or their exposure on the outer cell-membrane (on-cell catalysis).

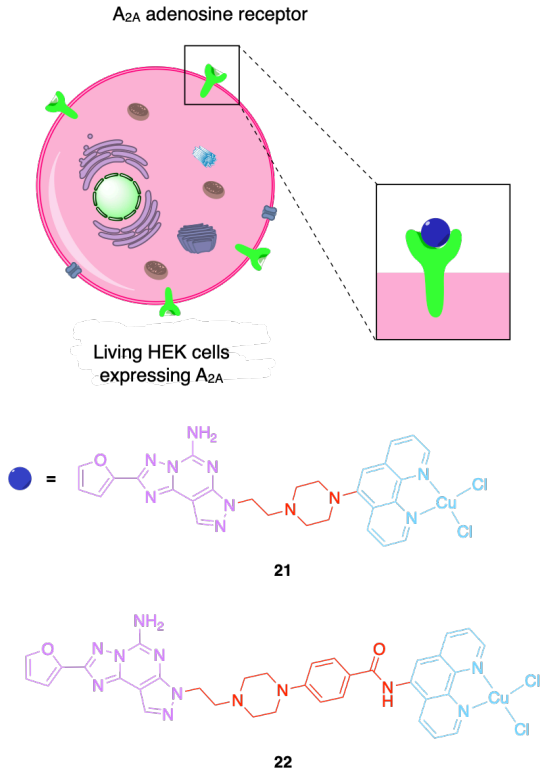

Figure 19. Artificial metalloenzymes based on the A_{2A} adenosine receptor embedded in the cytoplasmic membranes of living human cells. Trojan-horse molecules **21** and **22** presenting a catalytic center in blue, the spacer in red and the A_{2A} antagonist in violet.

Ghattas et al. prepared and characterized an artificial metalloenzyme based on the A_{2A} adenosine receptor embedded in the cytoplasmic membrane of living human cells.[105] For this, a Trojan horse strategy (see section 4.1) was followed to assemble the metalloenzyme by inserting into the receptor a strong antagonist covalently bound to copper(II)-1,10-phenanthroline *via* either a short or a long linker (**21** and **22** in Figure 19). The affinity of the receptor for the conjugates was in the nanomolar range as measured by competition with a radioligand. Additionally, the time of residence of antagonists in the receptor was estimated to be more than three days using a fluorescent microscopy approach *i.e.* imaging cells stained by a conjugate formed by a fluorescent probe covalently bound to the A_{2A} antagonist. The cells containing the receptor-complex conjugates were used to catalyze the abiotic DA cycloaddition of **8a-c** and CP. Results revealed that the longer conjugate (**22**) did not provide selectivity, which indicated that the complex might have protruded from the receptor binding pocket. The shorter conjugate (**21**) provided *ee* up to 28% as observed when starting from substrate **8c** and a maximum of 42% conversion which was observed when starting with substrate **8a**. This demonstrates that artificial metallo-DAases can indeed be used for *on-cell* catalysis. These results can be the basis of an exciting prospect for the organ-confined *in vivo* preparation of receptor-based artificial metalloenzymes for catalysis of exogenous reactions. These could be used for targeted synthesis by catalyzing cascades of reactions in concert with natural enzymes.[113]

4.6. Conclusion and perspectives

The simplest strategy to generate an artificial metalloenzyme consists in the “coordination strategy”, *e.g.* using amino acid side-chains to bind a metal cofactor, either introducing them by mutagenesis or using an already existing metal-binding site. Covalent anchoring of the complex leads to stable and precise positioning of the metal cofactor. One challenging issue of the latter strategy towards *in cell* catalysis lies in the use of orthogonal protein chemical tools allowing selective modification of the desired protein *in vivo* and non-natural amino-acids are certainly

important tools to achieve this goal.[114-116] Finally, supramolecular insertion of metallic cofactor was shown to be successful, but it is challenged by the intrinsic affinity that the protein must have for the metal complex, therefore limiting the panel of possible protein scaffolds and leaving the possibility of catalyst (or metal ion) release in case of low affinity. However, this strategy successfully provided metallo-DAases for *in cell* catalysis.[105]

One main difficulty in developing an artificial metalloenzyme is to find the appropriate scaffold and in many cases, the metal-containing artificial DAases (in absence of optimization) displayed lower selectivity as compared to other DAases. It has to be noted, though, that no optimization steps have been performed on metal-containing DAases. Beyond DA reaction, artificial metalloenzymes have been extensively developed to catalyze redox reactions for which a redox-active metal center is often required.[4,6,117-120] Although evolutionary strategies have been applied to optimize artificial metalloenzymes,[7,121-123] similar strategies have not been applied to metallo-DAases. To our opinion, this may be due to the fact that DA reaction was used to probe the selected scaffold, the cofactor's position within the cavity, constrains and flexibility around the substrates etc. Probably more importantly, this may be related to the limited substrate's scope. Indeed, most examples have been developed to catalyze the model reaction between CP and azachalcons, the latter providing a bidentate metal-binding motif. To extend the substrate's scope, a low affinity interaction between the substrate and the metal would be sufficient if combined with appropriately located second-coordination sphere residues to position the substrates. To this end, emerging tools for computationally designing metal sites in proteins should allow the generation of *De novo* designed metallo-DAases with extended substrates panel.[73]

Finally, efforts in the field have mainly relied on evaluating the properties of purified proteins as metal cofactors are often sensitive to cellular components. To overcome this limitation, it is important to develop strategies to protect the essential metal cofactors within the cellular environment, while avoiding metal release and side-reactions that could be deleterious to the living cells. Notably, recent examples of artificial metalloenzymes incorporated on or inside cells have recently been reported.[9,10,105,113,119]

5. General conclusions

Considering the current eco-conscious public and governmental movements, mastering biocatalysts is gaining importance and a growing number of biocatalysts with industrial applications have emerged. Although there are no industrial applications yet, artificial enzymes emerge as one main tool of the synthetic biology toolbox as they appear as essential to expand the repertoire of accessible chemical reactions to the biological world, allowing the catalysis of abiotic reactions under ecofriendly conditions.

Driven by the importance of DA cycloadditions in chemical synthesis, chemists have employed several strategies for the preparation of artificial DAases. Overall nice achievements were obtained with several examples of highly selective DAases, and even, in some cases, DAses providing the disadvantaged *exo* product with almost total stereoselectivity. Overall, it appears that the most efficient artificial DAase is **CE20** derived from *de novo* design strategy after several optimization steps.[65] This example emphasizes both the power of enzyme computational design and the requirement for catalyst optimization after the initial design. Recent progresses in directed evolution techniques[124-127] together with the development of more and more accurate computational tools[73] should allow improving the catalytic proficiency and stability of artificial enzymes, and many examples presented in this review should be considered as proof-of-concepts.

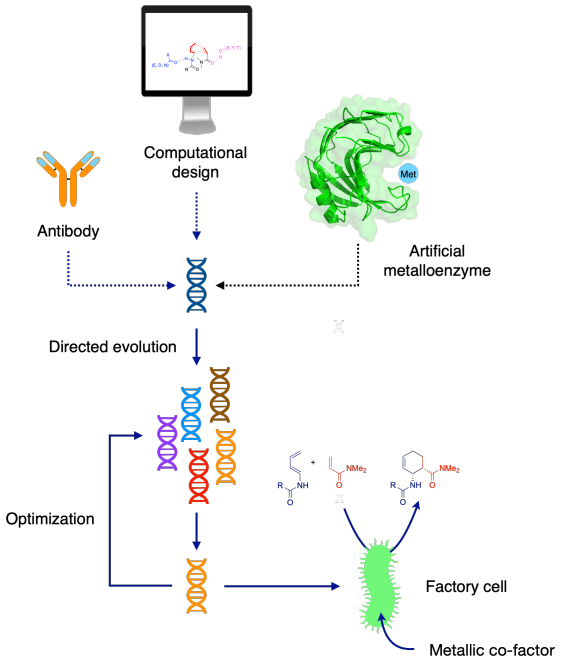

Figure 20. General strategies that can be followed to prepare an efficient artificial enzyme for *in vitro* or *in cell* applications.

In summary after selection of a target DA reaction, several strategies have been followed to prepare artificial enzymes which can be divided into two main approaches (Figure 20) *(i)* selecting or designing a protein that stabilizes the TS of the selected DA reaction (immunization or computational design) or *(ii)* selecting a protein cavity to accommodate a cofactor to catalyze the reaction. In the latter strategy, one main challenge is the choice of the cavity. As catalyst optimization appears as essential, fine-tuning of the selected cavity will be a crucial step towards the use of the second strategy. The optimized catalyst could then be inserted inside cells or on cells using tools ranging from genetic expression, protein delivery inside cells, or cell surface engineering. Beyond DA reaction, the above-mentioned strategies can be followed to develop artificial enzymes and implement a good number of abiological reactions into biocatalysis.

Wadih Ghattas obtained a PhD in bioinorganic chemistry at Aix Marseille University with Drs. A.J. Simaan and M. Réglier. He joined the group of Prof. M. Albrecht (University College Dublin) and then the group of Prof. C. E. Müller (Rheinische Friedrich Wilhelms Universität Bonn) for postdoctoral positions. He was awarded a "retour post-doctorant" grant from the "Agence Nationale de la Recherche" to develop artificial enzymes for *in vivo* catalysis at Paris-Saclay University, where he is now a CNRS researcher. His research focuses on the preparation of bio-inspired catalysts, chimeric enzymes and artificial enzymes for chemical synthesis or theragnostic tools.

Jean-Pierre Mahy prepared his thesis at the Ecole Nationale Supérieure de Chimie de Paris under the supervision of Drs. P. Battioni and D. Mansuy. He then joined the group of Prof. S.J. Benkovic at Pennstate University (USA) as post-doctoral fellow and started a new field of research concerning catalytic antibodies with a metalloporphyrin cofactor. He moved back to Paris as a CNRS researcher and was later appointed professor at Paris-Saclay University where he is director of a group which thematics are centered on the design of new metal complexes and the study of their interactions with biomolecules, in particular for the design of artificial metalloenzymes.

Marius Réglier is a CNRS Research Director Emeritus in Aix Marseille University. He prepared a PhD with Dr. S. Julia at Pierre and Marie Curie University in Paris. Following a two-year postdoctoral stay in the group of Prof. W. Oppolzer (University of Geneva) he moved to the Aix-Marseille University, where he started his own research group. He founded the BiosCiences laboratory, which focuses on the design and study of bio-inspired catalysts, artificial enzymes and hybrid catalysts as part of a reasoned development of new tools for chemical synthesis.

Ariane Jalila Simaan is a CNRS research director in Aix-Marseille University. She prepared her doctorate in bioinorganic chemistry in Paris XI University with Profs. J.-J. Girerd and F. Banse. She then joined the group of P. Hildebrandt (Max-Planck Institut in Mülheim-Ruhr/Gemany then ITQB in Lisboa/Portugal as postdoctoral fellow. She moved to Aix-Marseille University to carry on her own research centered on metal ions in biology with approaches ranging from bioinspired catalysis, enzymatic studies, hybrid catalysts and spectroscopic studies.

Keywords: Artificial enzymes • Diels-Alder • De novo design • catalytic antibody • artificial metalloenzyme

[1] J. Nielsen, J. D. Keasling, *Cell* **2016**, *164*, 1185–1197.
[2] C. J. Paddon, P. J. Westfall, D. J. Pitera, K. R. Benjamin, K. Fisher, D. McPhee, M. D. Leavell, A. Tai, A. Main, D. Eng, et al., *Nature* **2013**, *496*, 528–532.
[3] J. D. Keasling, *Science* **2010**, *330*, 1355–1358.
[4] K. Chen, F. H. Arnold, **2020**, *3*, 203–213.
[5] R. A. Sheldon, D. Brady, *ChemComm* **2018**, *54*, 6088–6104.
[6] F. Schwizer, Y. Okamoto, T. Heinisch, Y. Gu, M. M. Pellizzoni, V. Lebrun, R. Reuter, V. Köhler, J. C. Lewis, T. R. Ward, *Chem. Rev.* **2018**, *118*, 142–231.
[7] M. Jeschek, R. Reuter, T. Heinisch, C. Trindler, J. Klehr, S. Panke, T. R. Ward, *Nature* **2016**, *537*, 661–665.
[8] A. R. Grimm, D. F. Sauer, T. Polen, L. Zhu, T. Hayashi, J. Okuda, U. Schwaneberg, *ACS Catal.* **2018**, *8*, 2611–2614.
[9] T. Heinisch, F. Schwizer, B. Garabedian, E. Csibra, M. Jeschek, J. Vallapurackal, V. B. Pinheiro, P. Marlière, S. Panke, T. R. Ward, *Chem. Sci.* **2018**, *9*, 5383–5388.
[10] M. Szponarski, F. Schwizer, T. R. Ward, K. Gademann, *Communications Chemistry* **2018**, *1*, 84.
[11] O. Diels, K. Alder, **1928**, *460*, 98–122.
[12] K. C. Nicolaou, S. A. Snyder, T. Montagnon, G. Vassilikogiannakis, *Angew. Chem. Int. Ed. Engl.* **2002**, *41*, 1668–1698.
[13] J.-A. Funel, S. Abele, *Angew. Chem. Int. Ed. Engl.* **2013**, *52*, 3822–3863.
[14] B. L. Oliveira, Z. Guo, G. J. L. Bernardes, *Chem. Soc. Rev.* **2017**, *46*, 4895–4950.
[15] R. B. Woodward, R. Hoffmann, *Angew. Chem. Int. Ed. Engl.* **1969**, *8*, 781–853.
[16] K. N. Houk, *J. Am. Chem. Soc.* **1973**, *95*, 4092–4094.
[17] F. Gallier, *Curr. Org. Chem.* **2016**, *20*, 2222–2253.
[18] S. K. Mangawa, S. K. Awasthi, *Recent Advances in Organocatalysis* **2016**, 57–84.
[19] W. Blockziji, M. J. Blendamer, J. B. F. N. Engberts, *J. Am. Chem. Soc.* **1991**, *113*, 4241–4246.
[20] E. M. Gallego, C. Paris, Á. Cantín, M. Moliner, A. Corma, *Chem. Sci.* **2019**, *10*, 8009–8015.
[21] S. P. Kim, A. G. Leach, K. N. Houk, *J Org Chem* **2002**, *67*, 4250–4260.
[22] M. De Rosa, P. La Manna, C. Talotta, A. Soriente, C. Gaeta, P. Neri, *Front. Chem.* **2018**, *6*, 84.
[23] A. Palma, M. Artelsmair, G. Wu, X. Lu, S. J. Barrow, N. Uddin, E. Rosta, E. Masson, O. A. Scherman, *Angew. Chem. Int. Ed. Engl.* **2017**, *56*, 15688–15692.
[24] E. J. Corey, *Angew. Chem. Int. Ed. Engl.* **2002**, *41*, 1650–1667.
[25] B. Seelig, A. Jäschke, *Chem Biol* **1999**, *6*, 167–176.
[26] G. Roelfes, B. L. Feringa, *Angew. Chem. Int. Ed. Engl.* **2005**, *44*, 3230–3232.
[27] J. H. Yum, S. Park, H. Sugiyama, *Org Biomol Chem* **2019**, *17*, 9547–9561.
[28] G. Roelfes, *Mol Biosyst* **2007**, *3*, 126–135.
[29] N. Duchemin, I. Heath-Apostolopoulos, M. Smietana, S. Arseniyadis, *Org Biomol Chem* **2017**, *15*, 7072–7087.
[30] M. Smietana, S. Arseniyadis, *Chimia (Aarau)* **2018**, *72*, 630–634.
[31] K. Auclair, A. Sutherland, J. Kennedy, D. J. Witter, Van den Heever Johan P, C. R. Hutchinson, J. C. Vederas, *J. Am. Chem. Soc.* **2000**, *122*, 11519–11520.
[32] K. Watanabe, T. Mie, A. Ichihara, H. Oikawa, M. Honma, *J. Biol. Chem.* **2000**, *275*, 38393–38401.
[33] H. J. Kim, M. W. Ruszczycky, S.-H. Choi, Y.-N. Liu, H.-W. Liu, *Nature* **2011**, 1–4.
[34] A. Minami, H. Oikawa, *J. Antibiot.* **2016**, *69*, 500–506.
[35] B.-S. Jeon, S.-A. Wang, M. W. Ruszczycky, H.-W. Liu, *Chem. Rev.* **2017**, *117*, 5367–5388.
[36] C. T. Walsh, Y. Tang, *Biochemistry* **2018**, *57*, 3087–3104.
[37] B. R. Lichman, S. E. O'Connor, H. Kries, *Chem. Eur. J.* **2019**, *25*, 6864–6877.
[38] C. S. Jamieson, M. Ohashi, F. Liu, K. N. Houk, *Nat. Prod. Rep.* **2019**, *36*, 698–713.
[39] S. C. Farrow, M. O. Kamileen, L. Caputi, K. Bussey, J. E. A. Mundy, R. C. McAtee, C. R. J. Stephenson, S. E. O'Connor, *J. Am. Chem. Soc.* **2019**, *141*, 12979–12983.
[40] Q. Chen, J. Gao, C. Jamieson, J. Liu, M. Ohashi, J. Bai, D. Yan, B. Liu, Y. Che, Y. Wang, et al., *J. Am. Chem. Soc.* **2019**, *141*, 14052–14056.
[41] K. Cottet, M. Kolympadi, D. Marković, M.-C. Lallemand, *Curr. Org. Chem.* **2016**, *20*, 2421–2442.

[42] L. Gao, C. Su, X. Du, R. Wang, S. Chen, Y. Zhou, C. Liu, X. Liu, R. Tian, L. Zhang, et al., *Nat. Chem.* **2020**, 1–26.
[43] Y. Cai, Y. Hai, M. Ohashi, C. S. Jamieson, M. Garcia-Borras, K. N. Houk, J. Zhou, *Nat. Chem.* **2019**, *11*, 812–820.
[44] Q. Dan, S. A. Newmister, K. R. Klas, A. E. Fraley, T. J. McAfoos, A. D. Somoza, J. D. Sunderhaus, Y. Ye, V. V. Shende, F. Yu, et al., *Nat. Chem.* **2019**, *11*, 1–11.
[45] C. D. Fage, E. A. Isiorho, Y. Liu, D. T. Wagner, H.-W. Liu, A. T. Keatinge-Clay, *Nat. Chem. Biol.* **2015**, *11*, 256–258.
[46] M. J. Byrne, N. R. Lees, L.-C. Han, M. W. van der Kamp, A. J. Mulholland, J. E. M. Stach, C. L. Willis, P. R. Race, *J. Am. Chem. Soc.* **2016**, *138*, 6095–6098.
[47] Y. Guo, L. Yang, Z. Zhao, Z. Wu, H. Zhang, J. Liu, X. Cheng, J. Wu, H. Yang, H. Jiang, et al., *Cell Chem. Biol.* **2016**, *23*, 352–360.
[48] Y. Gong, Y. Guo, Z. Zhao, Z. Wu, Z. Zhou, D. Chen, L. Pan, *Cell Chem. Biol.* **2018**, *25*, 718–727.e3.
[49] M. I. Page, W. P. Jencks, *Proc. Natl. Acad. Sci. USA* **1971**, *68*, 1678–1683.
[50] Y. Xu, N. Yamamoto, *Bioorg Med Chem* **2004**, *12*, 5247–5268.
[51] D. Hilvert, K. W. Hill, K. D. Nared, M.-T. M. Auditor, *J. Am. Chem. Soc.* **1989**, *111*, 9262–9263.
[52] J. Xu, Q. Deng, J. Chen, K. N. Houk, J. Bartek, D. Hilvert, I. A. Wilson, *Science* **1999**, *286*, 2345–2348.
[53] J. Chen, Q. Deng, R. Wang, K. N. Houk, D. Hilvert, *ChemBioChem* **2000**, *1*, 255–261.
[54] A. C. Braisted, P. G. Schultz, *J. Am. Chem. Soc.* **1990**, *112*, 7431–7433.
[55] H. D. Ulrich, P. A. Patten, P. L. Yang, F. E. Romesberg, P. G. Schultz, *Proc. Natl. Acad. Sci. USA* **1995**, *92*, 11907–11911.
[56] F. E. Romesberg, B. Spiller, P. G. Schultz, R. C. Stevens, *Science* **1998**, *279*, 1929–1933.
[57] X. Zhang, Q. Deng, S. H. Yoo, K. N. Houk, *J Org Chem* **2002**, *67*, 9043–9053.
[58] V. E. Gouverneur, K. N. Houk, B. de Pascual-Teresa, B. Beno, K. D. Janda, R. A. Lerner, *Science* **1993**, *262*, 204–208.
[59] J. T. Yli-Kauhaluoma, J. A. Ashley, C.-H. Lo, L. Tucker, M. M. Wolfe, K. D. Janda, *J. Am. Chem. Soc.* **1995**, *117*, 7041–7047.
[60] A. A. P. Meekel, M. Resmini, U. K. Pandit, *J. Chem. Soc., Chem. Commun.* **1995**, *68*, 571–572.
[61] M. Resmini, A. A. P. Meekel, U. K. Pandit, *Pure Appl Chem* **1996**, *68*, 2025–2028.
[62] Y.-J. Hu, Y.-Y. Ji, Y.-L. Wu, B.-H. Yang, M. Yeh, *Bioorg Med Chem Lett* **1997**, *7*, 1601–1606.
[63] Z.-D. Shi, B.-H. Yang, Y.-L. Wu, Y.-J. Pan, Y.-Y. Ji, M. Yeh, *Bioorg Med Chem Lett* **2002**, *12*, 2321–2324.
[64] J. B. Siegel, A. Zanghellini, H. M. Lovick, G. Kiss, A. R. Lambert, J. L. St Clair, J. L. Gallaher, D. Hilvert, M. H. Gelb, B. L. Stoddard, et al., *Science* **2010**, *329*, 309–313.
[65] N. Preiswerk, T. Beck, J. D. Schulz, P. Milovník, C. Mayer, J. B. Siegel, D. Baker, D. Hilvert, *Proc. Natl. Acad. Sci. USA* **2014**, *111*, 8013–8018.
[66] C. B. Eiben, J. B. Siegel, J. B. Bale, S. Cooper, F. Khatib, B. W. Shen, F. Players, B. L. Stoddard, Z. Popovic, D. Baker, *Nat. Biotechnol.* **2012**, *30*, 190–192.
[67] A. Heine, E. A. Stura, J. T. Yli-Kauhaluoma, C. Gao, Q. Deng, B. R. Beno, K. N. Houk, K. D. Janda, I. A. Wilson, *Science* **1998**, *279*, 1934–1940.
[68] C. E. Cannizzaro, J. A. Ashley, K. D. Janda, K. N. Houk, *J. Am. Chem. Soc.* **2003**, *125*, 2489–2506.
[69] A. Zhao, M. R. Tohidkia, D. L. Siegel, G. Coukos, Y. Omidi, *Crit. Rev. Biotechnol.* **2014**, *36*, 276–289.
[70] R. J. Pantazes, M. J. Grisewood, C. D. Maranas, *Curr. Opin. Struc. Biol.* **2011**, *21*, 467–472.
[71] A. Zanghellini, *Curr. Opin. Biotech.* **2014**, *29*, 132–138.
[72] K. Świderek, I. Tuñón, V. Moliner, J. Bertran, *Arch. Biochem. Biophys.* **2015**, *582*, 68–79.
[73] V. Vaissier Welborn, T. Head-Gordon, *Chem. Rev.* **2019**, *119*, 6613–6630.
[74] P.-S. Huang, S. E. Boyken, D. Baker, *Nature* **2016**, *537*, 320–327.
[75] J. K. Lassila, H. K. Privett, B. D. Allen, S. L. Mayo, *Proc. Natl. Acad. Sci. USA* **2006**, *103*, 16710–16715.
[76] H. Fazelinia, P. C. Cirino, C. D. Maranas, *Protein Sci.* **2009**, *18*, 180–195.
[77] X. Zhu, L. Lai, *J. Comput. Chem.* **2009**, *30*, 256–267.
[78] Y. Lei, W. Luo, Y. Zhu, *Protein Sci.* **2011**, *20*, 1566–1575.
[79] C. Zhang, L. Lai, *Proteins* **2012**, *80*, 1078–1094.
[80] B. Kuhlman, *J. Biol. Chem.* **2019**, *294*, 19436–19443.
[81] A. Zanghellini, L. Jiang, A. M. Wollacott, G. Cheng, J. Meiler, E. A. Althoff, D. Röthlisberger, D. Baker, *Protein Sci.* **2006**, *15*, 2785–2794.
[82] B. Koepnick, J. Flatten, T. Husain, A. Ford, D.-A. Silva, M. J. Bick, A. Bauer, G. Liu, Y. Ishida, A. Boykov, et al., *Nature* **2019**, *570*, 1–19.
[83] A. Goldenzweig, S. J. Fleishman, *Annu. Rev. Biochem.* **2018**, *87*, 105–129.
[84] B. D. Weitzner, Y. Kipnis, A. G. Daniel, D. Hilvert, D. Baker, *Protein Sci.* **2019**, *28*, 2036–2041.
[85] T. Ose, K. Watanabe, H. Watanabe, M. Yao, H. Oikawa, I. Tanaka, *Nature* **2003**, *422*, 185–189.
[86] C. R. W. Guimarães, M. Udier-Blagović, W. L. Jorgensen, *J. Am. Chem. Soc.* **2005**, *127*, 3577–3588.
[87] A. Draksharapu, W. R. Browne, G. Roelfes, *Dalton Trans.* **2015**, *44*, 3656–3663.
[88] S. Otto, F. Bertoncin, *J. Am. Chem. Soc.* **1996**, *118*, 7702–7707.
[89] S. Otto, J. B. F. N. Engberts, *J. Am. Chem. Soc.* **1999**, *121*, 6798–6806.
[90] E. B. Mubofu, J. B. F. N. Engberts, *J. Phys. Org. Chem.* **2004**, *17*, 180–186.
[91] M. T. Reetz, N. Jiao, *Angew. Chem. Int. Ed. Engl.* **2006**, *45*, 2416–2419.
[92] W. Ghattas, L. Cotchico-Alonso, J.-D. Marechal, A. Urvoas, M. Rousseau, J.-P. Mahy, R. Ricoux, *ChemBioChem* **2016**, *17*, 433–440.
[93] P. J. Deuss, G. Popa, A. M. Z. Slawin, W. Laan, P. C. J. Kamer, *ChemCatchem* **2013**, *5*, 1184–1191.
[94] H. Osseili, D. F. Sauer, K. Beckerle, M. Arlt, T. Himiyama, T. Polen, A. Onoda, U. Schwaneberg, T. Hayashi, J. Okuda, *Beilstein J. Org. Chem.* **2016**, *12*, 1314–1321.
[95] M. Filice, O. Romero, J. Gutiérrez-Fernández, B. de las Rivas, J. A. Hermoso, J. M. Palomo, *ChemComm* **2015**, *51*, 9324–9327.
[96] J. Bos, F. Fusetti, A. J. M. Driessen, G. Roelfes, *Angew. Chem. Int. Ed. Engl.* **2012**, *51*, 7472–7475.
[97] T. Di Meo, W. Ghattas, C. Herrero, C. Velours, P. Minard, J.-P. Mahy, R. Ricoux, A. Urvoas, *Chem. Eur. J.* **2017**, *23*, 10156–10166.
[98] T. Di Meo, K. Kariyawasam, W. Ghattas, M. Valerio-Lepiniec, G. Sciortino, J.-D. Marechal, P. Minard, J.-P. Mahy, A. Urvoas, R. Ricoux, *ACS Omega* **2019**, *4*, 4437–4447.
[99] J. Podtetenieff, A. Taglieber, E. Bill, E. J. Reijerse, M. T. Reetz, *Angew. Chem. Int. Ed. Engl.* **2010**, *49*, 5151–5155.
[100] J. Fischer, D. Renn, F. Quitterer, A. Radhakrishnan, M. Liu, A. Makki, S. Ghorpade, M. Rueping, S. T. Arold, M. Groll, et al., *ACS Catal.* **2019**, *9*, 11371–11380.
[101] D. Coquiere, J. Bos, J. Beld, G. Roelfes, *Angew. Chem. Int. Ed. Engl.* **2009**, *48*, 5159–5162.

[102] W. Ghattas, V. Dubosclard, S. Tachon, M. Beaumet, R. Guillot, M. Réglier, A. J. Simaan, J.-P. Mahy, *Angew. Chem. Int. Ed. Engl.* **2019**, *58*, 14605–14609.
[103] T. Himiyama, D. F. Sauer, A. Onoda, T. P. Spaniol, J. Okuda, T. Hayashi, *J Inorg Biochem* **2016**, *158*, 55–61.
[104] T. Himiyama, N. Taniguchi, S. Kato, A. Onoda, T. Hayashi, *Angew. Chem. Int. Ed. Engl.* **2017**, *56*, 13618–13622.
[105] W. Ghattas, V. Dubosclard, A. Wick, A. Bendelac, R. Guillot, R. Ricoux, J.-P. Mahy, *J. Am. Chem. Soc.* **2018**, *140*, 8756–8762.
[106] A. Drevelle, M. Graille, B. Heyd, I. Sorel, N. Ulryck, F. Pecorari, M. Desmadril, H. van Tilbeurgh, P. Minard, *J Mol Biol* **2006**, *358*, 455–471.
[107] B. Talbi, P. Haquette, A. Martel, F. de Montigny, C. Fosse, S. Cordier, T. Roisnel, G. Jaouen, M. Salmain, *Dalton Trans.* **2010**, *39*, 5605–5607.
[108] X. A. Li, M. J. Sutcliffe, T. W. Schwartz, C. M. Dobson, *Biochemistry* **1992**, *31*, 1245–1253.
[109] M. Lerch, V. Gafner, R. Bader, B. Christen, G. Folkers, O. Zerbe, *J Mol Biol* **2002**, *322*, 1117–1133.
[110] N. El Bakkali-Taheri, S. Tachon, M. Orio, S. Bertaina, M. Martinho, V. Robert, M. Réglier, T. Tron, P. Dorlet, A. J. Simaan, *Arch. Biochem. Biophys.* **2017**, *623-624*, 31–41.
[111] G. De Simone, P. Ascenzi, F. Polticelli, *IUBMB Life* **2016**, *68*, 423–428.
[112] Y. M. Wilson, M. Dürrenberger, E. S. Nogueira, T. R. Ward, *J. Am. Chem. Soc.* **2014**, *136*, 8928–8932.
[113] Y. Okamoto, R. Kojima, F. Schwizer, E. Bartolami, T. Heinisch, S. Matile, M. Fussenegger, T. R. Ward, *Nat. Commun.* **2018**, *9*, 1943–1949.
[114] S. Smolskaya, Y. A. Andreev, *Biomolecules* **2019**, *9*, 255–17.
[115] K. J. Lee, D. Kang, H.-S. Park, *Mol. Cells* **2019**, *42*, 386–396.
[116] C. C. Liu, P. G. Schultz, *Annu. Rev. Biochem.* **2010**, *79*, 413–444.
[117] S. Bähr, S. Brinkmann-Chen, M. Garcia-Borras, J. M. Roberts, D. E. Katsoulis, K. N. Houk, F. H. Arnold, *Angew. Chem. Int. Ed. Engl.* **2020**, *2*, 1539–6.
[118] G. Roelfes, *Acc. Chem. Res.* **2019**, acs.accounts.9b00004.
[119] A. D. Liang, J. Serrano-Plana, R. L. Peterson, T. R. Ward, *Acc. Chem. Res.* **2019**, *52*, 585–595.
[120] C. Marchi-Delapierre, L. Rondot, C. Cavazza, S. Menage, *Isr. J. Chem.* **2014**, *55*, 61–75.
[121] R. K. Zhang, D. K. Romney, S. J. Kan, F. H. Arnold, in *Artificial Metalloenzymes and MetalloDNArtzymes in Catalysis From Design to Applications* (Eds.: M. Diéguez, J.-E. Bäckvall, O. Pàmies), Wiley-VCH Verlag GmbH & Co. KGaA, **2018**, pp. 137–170.
[122] I. D. Petrik, J. Liu, Y. Lu, *Curr. Opin. Chem. Biol.* **2014**, *19*, 67–75.
[123] M. T. Reetz, *Acc. Chem. Res.* **2019**, *52*, 336–344.
[124] K. K. Yang, Z. Wu, F. H. Arnold, *Nat. Meth.* **2019**, *16*, 687–694.
[125] R. Chowdhury, C. D. Maranas, *AIChE J* **2019**, *66*, 1110–17.
[126] U. Markel, K. D. Essani, V. Besirlioglu, J. Schiffels, W. R. Streit, U. Schwaneberg, *Chem. Soc. Rev.* **2020**, *49*, 233–262.
[127] G. Qu, A. Li, C. G. Acevedo-Rocha, Z. Sun, M. T. Reetz, *Angew. Chem. Int. Ed. Engl.* **2020**, *53*, 3916–29.